P.N. Lebedev Physical Institute of the Russian Academy of Sciences

3. Results of Flight Scientific Programmes, Research and Observation Realized (Implemented) in 2014-2015

RadioAstron Space VLBI Interferometer project: scientific results achieved in 2014-2015

1. Project description

RadioAstron is a space VLBI Mission aimed at achieving the highest angular resolution of radio observations at centimeter wavelengths through ground-space interferometric measurements on baselines of up to ~360,000km. The Mission consists of a 10-metre space-borne radio telescope (SRT) operating at wavelengths of 92, 18, 6.2, and 1.2–1.6 cm and supported by a range of ground-based facilities.

Basic parameters of the SRT and RadioAstron observations are summarized in Table 1 RadioAstron provides observations of radio sources at ultra-high angular resolution, with ground-space baselines of up to 360,000km reaching a resolution of about 7 microarcseconds at the wavelength of 1.3 cm. These observations enable accurate measurements of structural properties and evolution on sub-milliarcsecond scales in galactic and extragalactic radio sources. At intermediate baselines, high quality imaging of radio sources with moderate resolution can be obtained for objects located near the orbital plane or observed near perigee passages of the satellite.

Table 1

Observing bands (см)	Frequency range (MHz)	Smallest spacing (uas)	SEFD (kJy) LCP RCP		Baseline Sensitivity (mJy)
92 (P)	316-332	530	13.3	13.5	14
18 (L)	1636-1692	100	2.76	2.93	3
6.2 (C)	4804-4860	35	11.6	-	5
1.2-1.6 (K)	18372-25132	7	46.7	36.8	16

K-band observing can be done at one of the eight central frequencies: 18392, 19352, 20312, 21272, 22232, 23192, 24152, 25112 MHz. The fringe spacing is calculated for the longest possible baseline. The one-sigma baseline sensitivity is estimated for the RadioAstron–GBT pair for a 300 s integration time and 16 MHz bandwidth of a single polarization single frequency channel (IF).

The RadioAstron Mission is headed by the Astro Space Center (ASC) of the P.N. Lebedev Physical Institute in Moscow, Russia. The Spektr-R satellite operations are supported by the Russian Space Agency (RSA) “Roscosmos” and conducted by the Lavochkin Association (LA) in Chimki, Russia. Orbit determination measurements and analysis are performed by the Ballistics Group at the Keldysh Institute of Applied Mathematics (KIAM) in Moscow. Data from the SRT are received at the Pushchino STS operated by the ASC and the Green Bank STS operated by NRAO. The data from the SRT are recorded in the RadioAstron Data Format (RDF) specially developed for the Mission operations. Data correlation from RadioAstron observations is conducted at the RadioAstron Correlator Facility designed and operated at the Data Processing Department of the ASC. The MPIfR-DiFX software correlator and the EVN software correlator at JIVE (SFXC) are also being used to correlate RadioAstron experiments. Block time commitments to RadioAstron observations are being organized or considered at many GRT facilities.

Scientific operations of the RadioAstron Mission are conducted by the ASC and the radio interferometric networks. The RadioAstron International Science Council (RISC), which is comprised of representatives from the ASC, major GRT facilities, and the radio astronomical community, provides overall policy definitions for the Mission, and discusses scientific issues and priorities

There are a number of different ground facilities participating in operation, tracking, data transfer and observations with the radio antenna on board Spektr-R. These include the Flight Control Center (FCC) at the Lavochkin Association; the Deep Space Network Communication (DSNC) antennas in Ussurijsk and Bear Lakes employed for the uplink and telemetry communications with the satellite; the Satellite Tracking Station (STS) in Pushchino, Russia, and Green Bank, USA, used for telemetry and data acquisition from the Spektr-R satellite and radio antenna; the laser ranging stations (LRS) used for orbit determination measurements; and the ground radio telescopes (GRTs) taking part in Very Long Baseline Interferometry (VLBI) observations with the Spektr-R antenna (hereafter, RadioAstron observations). VLBI methods are being utilized to determine the space craft state vector for orbit reconstruction.

The scientific program of RadioAstron consists of three major parts: the Early Science Program (ESP), Key Science Program (KSP), and General Observing Time (GOT) projects. The Early Science Program, which finished in June 2013, explored the main scientific capabilities of RadioAstron observations and paved the way for the subsequent KSP and GOT programs. RadioAstron KSP observations commenced in July 2013. The KSP is aimed specifically at focusing on the areas of strongest scientific impact of RadioAstron and ensuring a long-lasting scientific impact for the Mission. KSP observations within the AO-1 peirod were carried out between July 2013 and June 2014, inclusive, and had a shared-risk nature since a number of observing modes were not fully tested by the ASC.

2. Science program of the mission in 2014-2015 years

Science program of the mission was formed on the basis of open competition between proposals submitted in response to Announcement of Opportunity (AO2 and AO3). There are no restrictions imposed on the nationality or affiliation of primary investigators and co-investigators of RadioAstron proposals. The RISC has formed a review panel to grade all proposals received — the RadioAstron Program Evaluation Committee (RPEC). RPEC consists of the following members: Richard Porcas (chairman) (MPIfR Bonn, Germany), Dave Jauncey (CSIRO, Australia), Mat Lister (PREDU, USA), Mikhail Popov (ASC FIAN, Russia), Jason Hessel (University of Amsterdam, The Netherlands), and Vouter Vlemmings (ONSALA Observatory, Sweden). Proposals submitted for observations with RadioAstron are reviewed separately by the RPEC and the requested ground facilities. It was approved 25 proposals for the period of AO2-AO3. Corresponding science program was developed for the period including 2014-2015 years.

There are three main scientific area covered by the RadioAstron mission: active galactic nuclei (AGN), pulsars and maser emission from star formation regions in our Galaxy and other galaxies. Ground support was provided by many large radio telescopes round the world located in Russia, Australia, Great Brirain, Germany, Spain, Italy, USA, Japan, India, China, Sweden, South Africa, and others. Successful results were achieved in all above mentioned areas. Main scientific results will be reviewed in present report, RadioAstron publications can be found from the following collection: http://www.asc.rssi.ru/radioastron/publications/publ.html

3. AGN studies

3.1. RadioAstron observations of the quasar 3C273: A challenge of the brightness temperature limit

Inverse Compton cooling limits the brightness temperature of the radiating plasma to a maximum of $10^{11.5}$ K. Relativistic boosting can increase its observed value, but apparent brightness temperatures much in excess of 10^{13} K are inaccessible using ground-based very long baseline interferometry (VLBI) at any wavelength. We present observations of the quasar 3C 273, made with the space VLBI mission RadioAstron on baselines up to 171,000 km, which directly reveal the presence of angular structure as small as 26 μas (2.7 light months) and brightness temperature in excess of 10^{13} K. These measurements challenge our understanding of the non-thermal continuum emission in the vicinity of supermassive black holes and require a much higher Doppler factor than what is determined from jet apparent kinematics.

Besides 3C273, brightness temperature is measured for many other sources within RadioAstron AGN survey. Up to date, 150 quasars have been detected at ground-to-space baselines. The brightness temperature of their cores is measured to be up to 10^{14} K and even higher – inconsistent with previous and current findings of ground-based VLBI surveys.

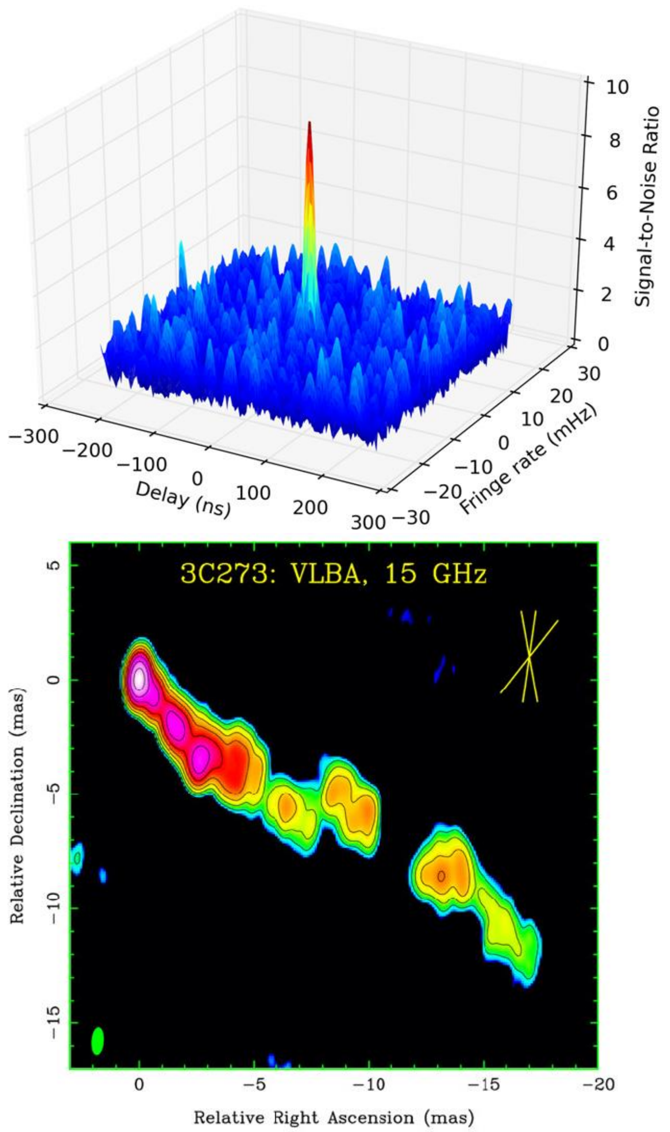

Fig. 3.1. *Left*: RadioAstron (Space Radio Telescope–GBT) 22 GHz interferometer response from observations of the quasar 3C 273 on 2013 February 2 with a projected baseline of 7.6 Gλ. The ratio of interferometer fringe amplitude to the average noise amplitude is shown as a function of the residual delay (in nanoseconds) and fringe rate (in millihertz). *Right*: Results of ground-based VLBA observations of the quasar 3C 273 made at 15 GHz (top, 2013 February 10, peak intensity 3.2 Jy/beam, noise level 1.4 mJy/beam, beam size 1.21×0.53 mas) Total intensity pseudo-color and contour image with the beam shown at the half power level in green. Contours start at 0.25% of the peak intensity and are plotted with ×2 steps at 15 GHz. The yellow lines show the range of position angles of ground-to-space RadioAstron baselines covered by our observations: 10°, −8°, −38°.

3.2. Extreme brightness temperatures and refractive substructure in 3C273 with RadioAstron.

Earth–space interferometry with RadioAstron provides the highest direct angular resolution ever achieved in astronomy at any wavelength. RadioAstron detections of the classic quasar 3C 273 on interferometric baselines up to 171,000 km suggest brightness temperatures exceeding expected limits from the “inverse-Compton catastrophe” by two orders of magnitude. We show that at 18 cm, these estimates most likely arise from refractive substructure introduced by scattering in the interstellar medium. We use the scattering properties to estimate an intrinsic brightness temperature of 7×10^{12} K, which is consistent with expected theoretical limits, but which is ~15 times lower than estimates that neglect substructure. At 6.2 cm, the substructure influences the measured values appreciably but gives an estimated brightness temperature that is comparable to models that do not account for the substructure. At 1.35 cm, the substructure does not affect the extremely high inferred brightness temperatures, in excess of 10^{13} K . We also demonstrate that for a source having a Gaussian surface brightness profile, a single long baseline estimate of refractive substructure determines an absolute minimum brightness temperature, if the scattering properties along a given line of sight are known, and that this minimum accurately approximates the apparent brightness temperature over a wide range of total flux densities.

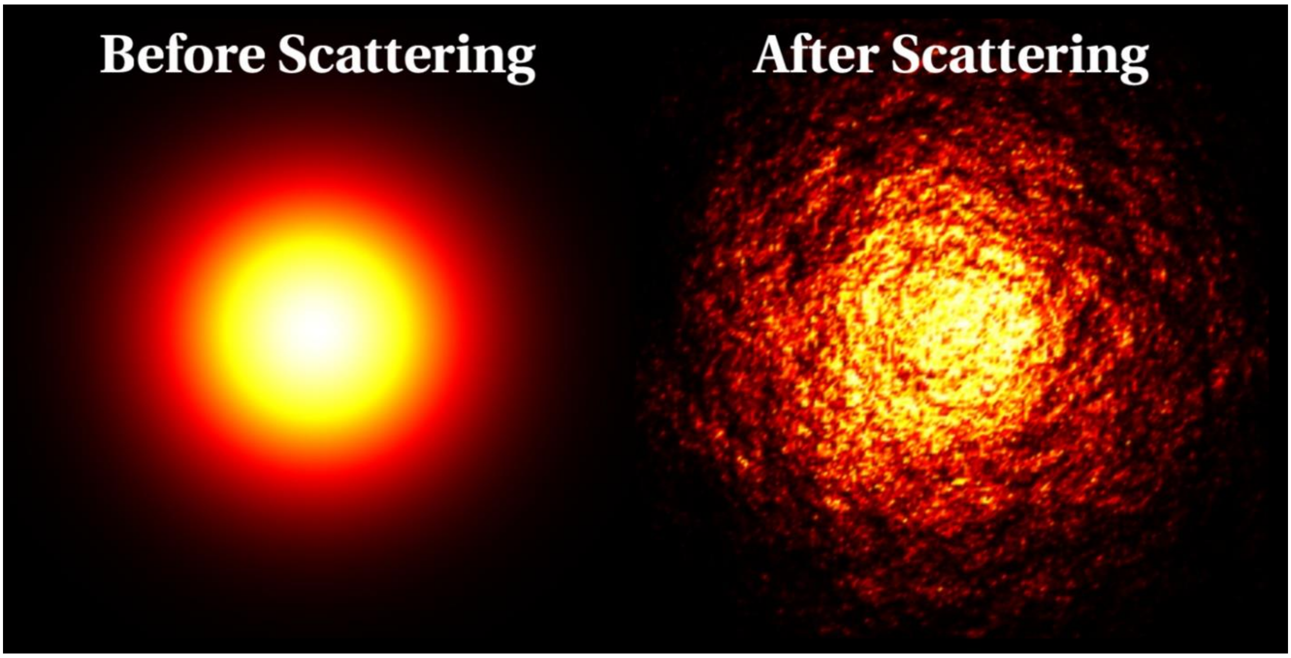

Fig. 3.2. Simulated images showing the effects of refractive substructure.

3.3. Probing the innermost regions of AGN jets and their magnetic fields with RadioAstron. Imaging BL Lacertae at 21 μas resolution

We present the first polarimetric space very long baseline interferometry (VLBI) imaging observations at 22 GHz. BL Lacertae was observed in 2013 November 10 with the RadioAstron space VLBI mission, including a ground array of 15 radio telescopes. The instrumental polarization of the space radio telescope is found to be less than 9%, demonstrating the polarimetric imaging capabilities of RadioAstron at 22 GHz. Ground–space fringes were obtained up to a projected baseline distance of 7.9 Earth diameters in length, allowing us to image the jet in BL Lacertae with a maximum angular resolution of 21 μas, the highest achieved to date. We find evidence for emission upstream of the radio core, which may correspond to a recollimation shock at about 40 μas from the jet apex, in a pattern that includes other recollimation shocks at approximately 100 and 250 μas from the jet apex. Polarized emission is detected in two components within the innermost 0.5 mas from the core, as well as in some knots 3 mas downstream. Faraday rotation analysis, obtained from combining RadioAstron 22 GHz and groundbased 15 and 43 GHz images, shows a gradient in rotation measure and Faraday-corrected polarization vector as a function of position angle with respect to the core, suggesting that the jet in BL Lacertae is threaded by a helical magnetic field. The intrinsic de-boosted brightness temperature in the unresolved core exceeds 3×10^{12} K, suggesting, at the very least, departure from equipartition of energy between the magnetic field and radiating particles.

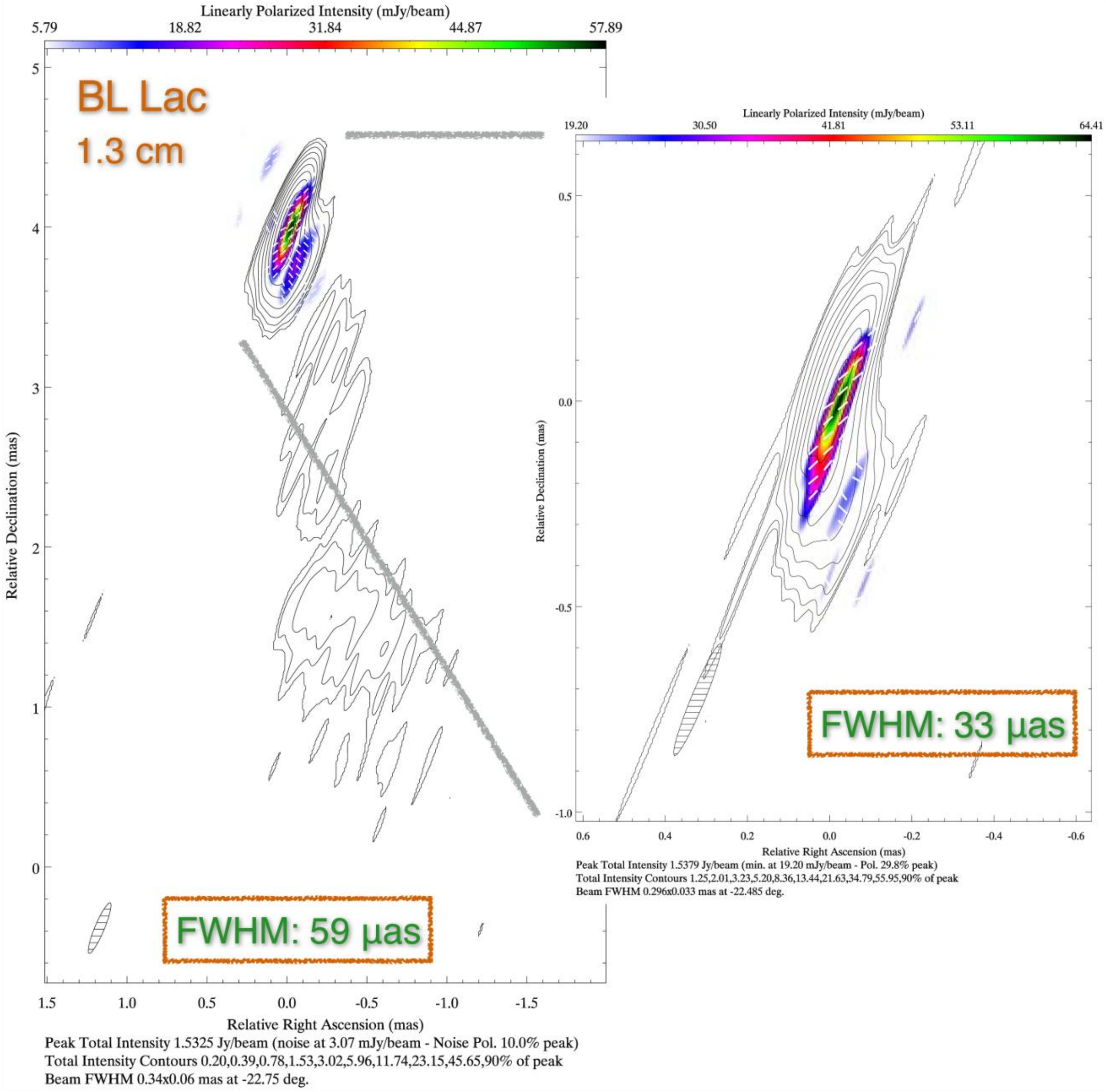

Fig.3.3. *RadioAstron polarimetric space VLBI images of BL Lac obtained in 2013 November 10–11 at 22 GHz with natural (left) and "super"-uniform (right) weightings.*

3.4 RadioAstron space VLBI imaging of polarized radio emission in the high-redshift quasar 0642+449 at 1.6 GHz.

Polarization of radio emission in extragalactic jets at a sub-milliarcsecond angular resolution holds important clues for understanding the structure of the magnetic field in the inner regions of the jets and in close vicinity of the supermassive black holes in the centers of active galaxies. Space VLBI observations provide a unique tool for polarimetric imaging at a sub-milliarcsecond angular resolution and studying the properties of magnetic field in active galactic nuclei on scales of less than 104 gravitational radii.

A space VLBI observation of high-redshift quasar TXS 0642+449 (OH 471), made at a wavelength of 18 cm (frequency of 1.6 GHz) as part of the early science programme (ESP) of the RadioAstron mission, is used here to test the polarimetric performance of the orbiting Space Radio Telescope (SRT) employed by the mission, to establish a methodology for making full Stokes polarimetry with space VLBI at 1.6 GHz, and to study the polarized emission in the target object on sub-milliarcsecond scales.

Polarization leakage of the SRT at 18 cm is found to be within 9% in amplitude, demonstrating the feasibility of high fidelity polarization imaging with RadioAstron at this wavelength. A polarimetric image of 0642+449 with a resolution of 0.8 mas (signifying an ~4 times improvement over ground VLBI observations at the same wavelength) is obtained. The image shows a compact core-jet structure with low (≈2%) polarization and predominantly transverse magnetic field in the nuclear region. The VLBI data also uncover a complex structure of the nuclear region, with two prominent features possibly corresponding to the jet base and a strong recollimation shock. The maximum brightness temperature at the jet base can be as high as 4×10^{13} K.

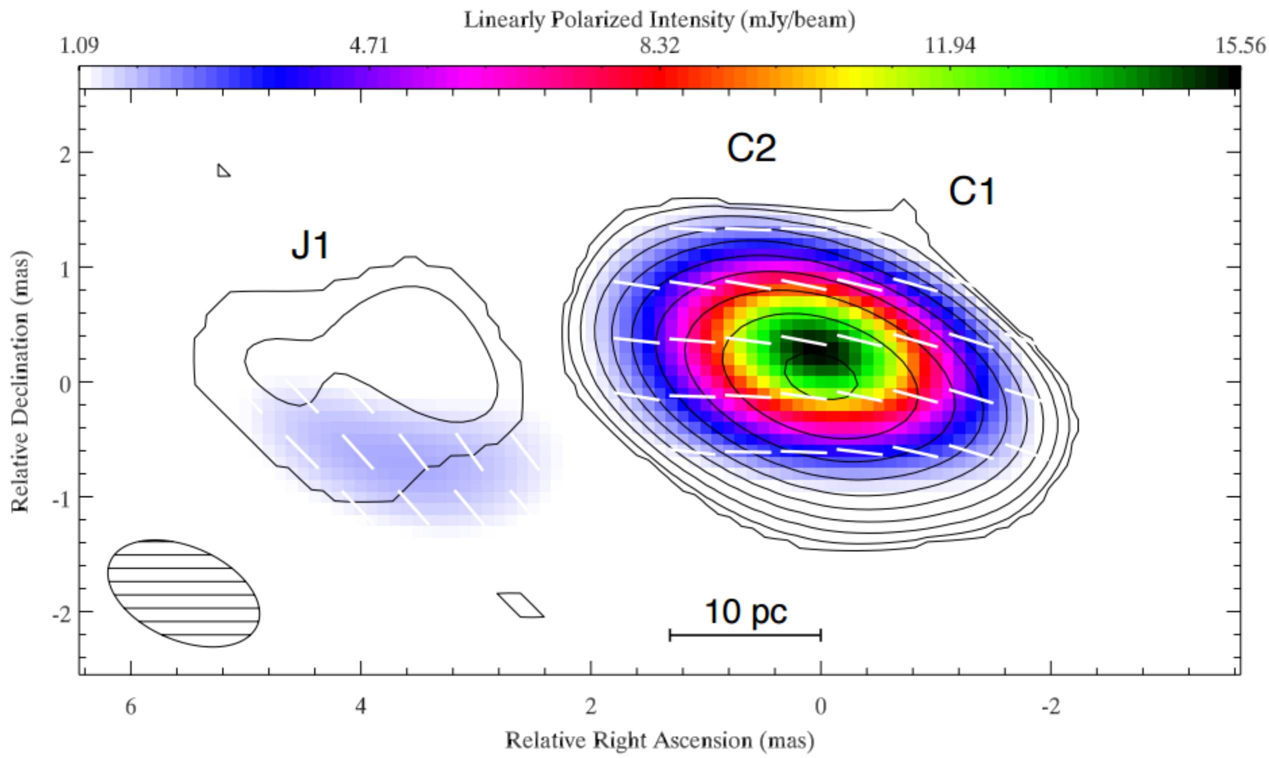

Fig. 3.4. *RadioAstron space VLBI image of 0642+449 of total (contours) and linearly polarized (color shades) emission, made using the uniform data weighting. The orientation of linear polarization is indicated by vectors.*

3.5. Ultra-high spatial resolution image of nearby radio galaxy 3C 84 at 22 GHz

The RadioAstron Key Science Program on imaging nearby active galactic nuclei has successfully produced an ultra-high spatial resolution space-VLBI image of 3C 84, a radio source located in the giant elliptical galaxy NGC 1275 in the Perseus Cluster at a distance of 75 Mpc. At this distance, an angular size of 1 milliarcsecond corresponds only to ~ 0.3 parsec linear size. Because of its proximity and bright, relatively compact radio emission, 3C 84 is one of the best candidates for studying the inner jet at very high spatial resolution and it was selected as an ideal target for space-VLBI imaging with RadioAstron. The ultra-high resolution images of 3C 84 will help us to understand the AGN jet formation and evolution within the innermost parsec from the central engine.

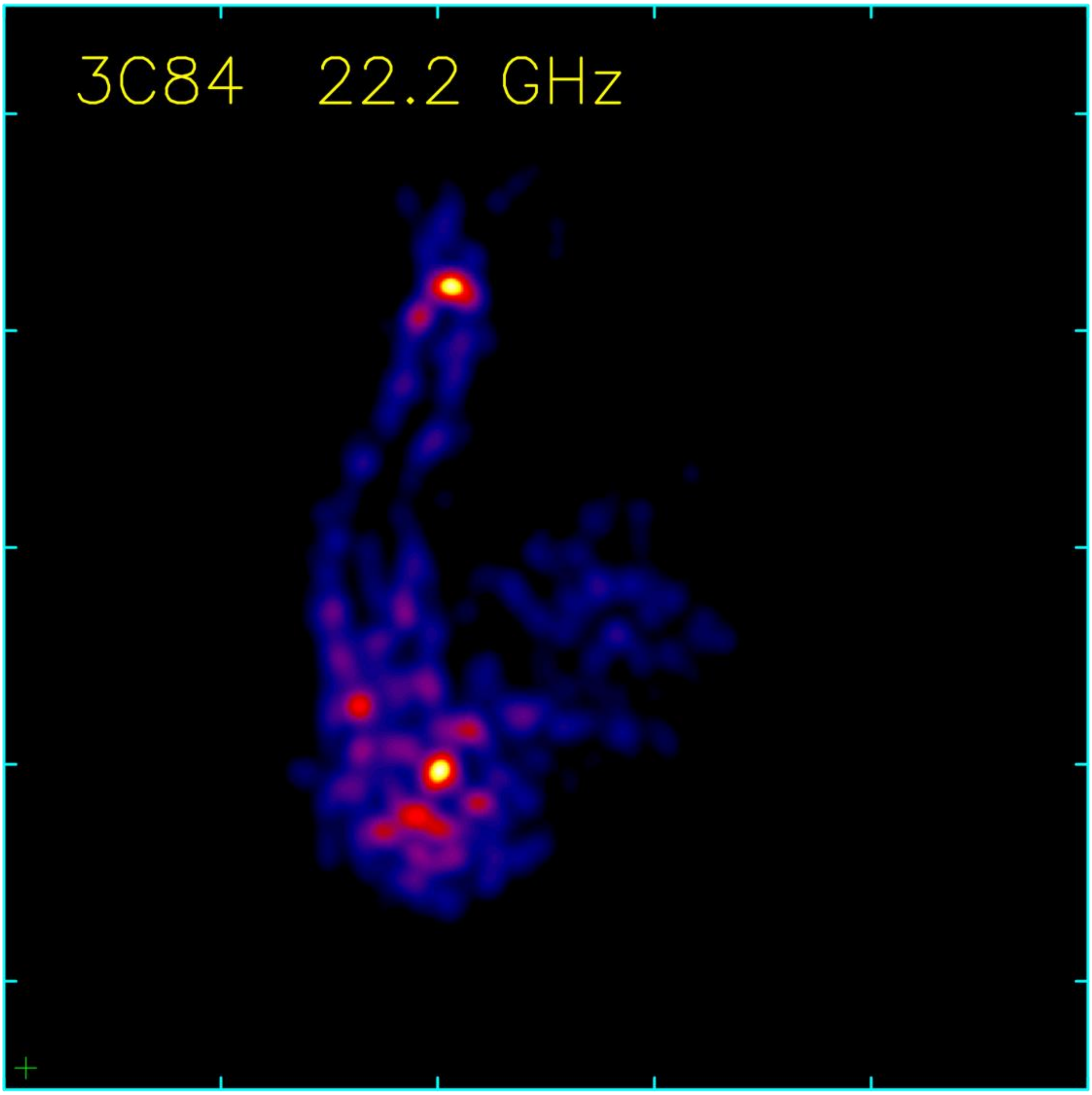

Fig. 3.5. RadioAstron total intensity image of a nearby radio galaxy 3C 84 at 22 GHz. The restoring beam size is 150 x 70 μas at an angle of 21 deg (shown in the lower left corner). The peak flux density is 1 Jy/beam. Tick marks have a 1 mas separation. The whole North-South extent of the visible jet structure is just ~ 1.2 pc in linear scale (projected).

The 22-hour long imaging experiment was carried out on 21-22 September 2013. Observations were obtained at the same time at 5 and 22 GHz using the dual-band observing mode of the Space Radio Telescope. The ground array data comes from 25 telecopes including the European VLBI Network together with the Russian Kvazar network, the Korean VLBI Network, Kalyazin and the NRAO telescopes Very Long Baseline Array, the Green Bank Telescope, and the phased Very Large Array. Part of the ground array observed at 5 GHz and a part at 22 GHz with Effelsberg switching between the two. The data presented here were correlated at the Max-Planck-Institut fur Radioastronomie, Bonn. Space-to-ground fringes were detected from 0.2 Earth Diameters (ED) up to ~ 7 ED at both frequencies. The Figure 3.5 shows the resulting 22 GHz space-VLBI image after the full data calibration and deconvolution.

At sub-mas scale, the central region of 3C 84 is resolved in a complex structure. The most prominent features are the core at the northern end of the jet and a bright component South of the core, which moves at sub-luminal speed along a curved trajectory connected to the core by a limb-brightened jet. The RadioAstron image shows substructure in these features at an unprecedented detail. For the first time a counter-jet is clearly visible at sub-parsec scale. The core is elongated in East-West direction implying a resolved structure at the angular resolution of about 50 μas, corresponding to about 500 Schwarzschild radii. The limb-brightened, well resolved jet and counter-jet can be seen right from the beginning. The bright spot inside the southern component is identified with the end of the limb-brightened jet. Its compactness indicates a very high brightness which is unusual for sub-luminal jets being observed at a large angle.

4.Pulsar studies

4.1. Probing cosmic plasma with giant pulses from the Crab pulsar

Giant pulses (GP) from Crab pulsar (B0531+21) were observed in RadioAstron project to study interstellar scattering effects. Nine observations were conducted during the period from 2011 to 2015. The list of these observations is shown in Table 1. Fringes at baseline up to 150 000 km were detected for the first time in radio interferometry of giant pulses from the Crab pulsar during joint space-ground observations with RadioAstron. Maximum peak flux density of detected giant pulses was about 100000 Jy. Scattering parameters were measured for each epoch of observation: scattering time, decorrelation bandwidth, angular size of scattering disk, diffraction radius, and distance to the effective scattering screen. Additionally, phase structure functions in time were analyzed. Measurement of all these parameters was done in assumption of single thin scattering screen model.

It was found that distance to the scattering screen for each epoch of observation has different value. In case of the first observations (RAFS01) the distance to the scattering screen corresponds to the case of homogeneous distribution of scattering material on the line of sight d=D/3. In other cases, it is seen that the scattering was dominating in the vicinity of Crab nebula.

Previous studies have already shown such two components scattering, which consists of the scattering located close to the nebula and the extended part, corresponding to the ISM. For example, Ramesh Karuppusamy showed in his work, that during the six hour observations of Crab pulsar, variations in scattering were observed in the Crab nebula, and these variations were originated in the vicinity of nebula.

Table 4.1. List of observations of pulsar B0531+21, conducted within the RadioAstron scientific program from 2011 to 2015.

Obs. Code	Date	Time	T, (hours)	⍰, (cm)	D, (km)	N_{GRT}	Corr. w
RAFS01	14.11.2011	23:00-00:00	1.0	18	46000	4	Y
RAES04A	02.03.2012	13:00-17:00	4.0	18	145000	8	
RAES04B	06.03.2012	13:30-17:30	4.0	18	128000	8	Y
RAES04D	23.10.2012	07:00-09:00	2.0	18	113000	7	Y
RAKS02AD	27.10.2013	06:00-09:00	3.0	18	150000	4	Y
RAKS02AE	02.11.2013	19:30-08:40	12.0	92	57000	5	
RAGS10A	10.01.2015	22:00-04:00	6.0	18	153000	5	Y
RAGS10B	28.01.2015	21:00-03:00	6.0	18/92	140000	10	Y
RAGS10C	15.02.2015	20:00-02:00	6.0	92	107000	2	

Additionally, numerical simulations of giant pulses scattering was performed with a given structure of GP through the scattering medium with a given characteristics (decorrelation bands). This approach allowed us to consider the influence of the characteristic giant pulses structure on the measured decorrelation band and the visibility function. Observed quasi-regular structure in visibility functions for individual giant pulses indicates the presence in the structure of these pulses of strong unresolved components at a frequency of 1668 MHz. These components were previously observed only at frequencies above 5 GHz, where they are not smeared by scattering. Thus, VLBI observations of giant pulses from Crab pulsar allowed us to postulate the presence in fine structure of these pulses unresolved bursts with duration of less than 30 ns and with the brightness temperature $T_b > 10^{38}$ K. Therefore, we conclude that such unresolved components with such high values of brightness temperature will act as strong electromagnetic waves, accelerating plasma particles, resulting in the formation of new components of radio emission in the pulsar profile: HFIP, HFC1, HFC2 discovered by Hankins.

Obtained results of our measurements are accumulated in Table 4.2.

Table 4.2. Table of measured scattering parameters.

Obs. code	$\square_{SC}$, (µs)	□, (mas)	□□, (kHz)	R_{diff}, (km)	□	Number G
RAFS01	0.9 ± 0.1	1.3 ± 0.2	116.3 ± 24.5	10361 ± 1700	0.36 ± 0.08	
RAES04A	5.8 ± 0.3	0.6 ± 0.1	55.2 ± 5.9	21817 ± 2900	0.94 ± 0.02	12
RAES04B	5.5 ± 0.7	0.5 ± 0.1	41.2 ± 7.9	26949 ± 7700	0.96 ± 0.03	10

RAES04D	5.1 ± 0.5	1.2 ± 0.1	40.7 ± 4.6	11413 ± 900	0.79 ± 0.03	9
RAKS02AD	2.2 ± 0.3	1.2 ± 0.1	78.1 ± 7.9	12113 ± 1200	0.61 ± 0.06	4
RAKS02AE	2340 ± 23	14.0 ± 1.4	–	5140 ± 500	0.92 ± 0.07	5
RAGS10A	1.4 ± 0.2	0.4 ± 0.1	161.1 ± 13.4	34015 ± 9268	0.91 ± 0.05	18
RAGS10B	1.5 ± 0.1	0.5 ± 0.1	70.2 ± 8.3	25675 ± 4485	0.85 ± 0.04	6
RAGS10C	–	–		–	–	

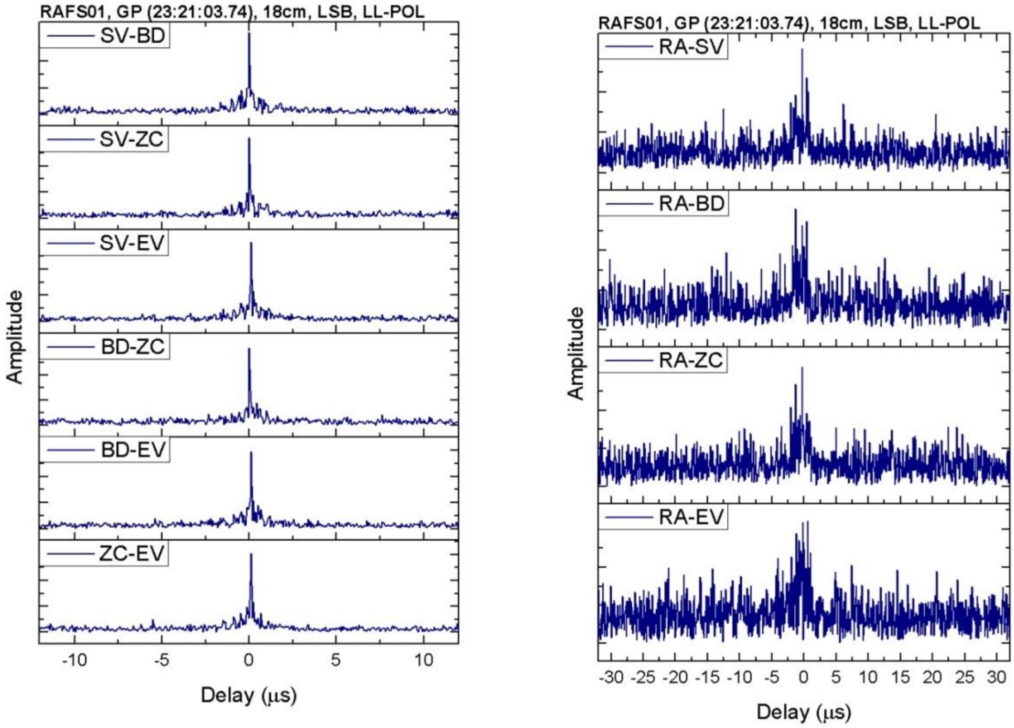

Fig. 4.1. Visibility functions for individual giant pulse for different baselines: ground baselines (left), space-ground baselines (right), observation code RAFS01, pulse: 23:21:03.74, 18 cm wavelength.

4.2. Distribution of inhomogeneities of the interstellar plasma in the direction to distant pulsars

Radio emission from astronomical sources is subjected to scattering on inhomogeneities of interstellar plasma. Scattering effects are the most pronounced for compact radio sources such as pulsars. After discovery of pulsars these effects were studied extensively theoretically and by observations. Main scattering effects are: angular broadening, pulse broadening, intensity scintillation, and frequency modulation of radio spectra.

Simultaneous measurements of such scattering effects during a sufficiently long time and in a broad frequency band enable us to obtain important information about structure of the interstellar plasma along the line of sight to the pulsar. Great advantage in this study brings the VLBI (very large baseline interferometry) observations, providing direct measurements of the angular broadening, namely, angular size of the scattering disk. New prospects in this direction provide space-ground interferometer RadioAstron with its angular resolution of 1 mas at 92 cm, and 0.2 mas at 18 cm.

Interferometric response or visibility $V_{AB}(\upsilon,t)$ in the domain of frequency is the product of electric fields at two telescopes. The representation of the visibility is known as the cross spectrum. Usually visibility is averaged over multiple accumulations of the spectrum to reduce noise. An inverse Fourier transform of υ to delay τ leads to the visibility $V_{AB}(\tau,t)$, and a forward Fourier transform of t to fringe rate f leads to $V_{AB}(\tau,f)$, which we call delay/fringe-rate diagram. If there were no scattering material between the pulsar and the observer, one would expect for the modulus of $V_{AB}(\tau,f)$ to manifest one notable spike at zero delay and fringe rate. Scattering material changes this picture, instead of single spike there is a spot of increased amplitude. This spot (scattering disk) was for the first time resolved with space-ground interferometer RadioAstron. Delay/fringe rate diagram is shown in Fig.4.3 for the pulsar B0329+54. Figure 4.2 presents evolution of the visibility function with increasing baseline projection of the interferometer. In fact, this is a cross-section through the maximum in the delay/fringe-rate diagram, which represents the visibility averaged over time span ΔT, that is equivalent to the integration time.

Fig. 4.2. Examples of the structure of the magnitude of visibility $V_{AB}(\tau,f_{max})$ as a function of delay τ, with fringe rate fixed. From the lowermost to uppermost, the curves correspond to progressively longer baselines, with the telescopes indicated and the approximate baseline projections given in Mλ in parentheses. Curves are offset vertically, and the upper two are magnified as the vertical scale indicates, for ease of viewing. For baseline projections greater than 30 Mλ, central spike vanished, and substructure in the scattering disk is seen.

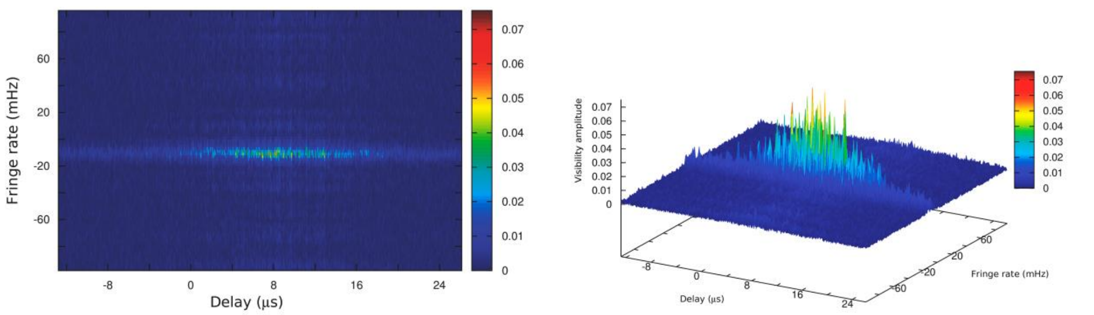

Fig. 4.3. Magnitude of visibility in the delay/fringe-rate domain for 500 s time span for PSR B0329+54 observed with Green Bank telescope (GBT) and RadioAstron on November 29 2012 with baseline projection of 235000 km. Right: three-dimensional representation; left: two-dimensional representation.

At relatively small baseline projections visibility function keeps the spike with amplitude decreasing with increasing baseline projection, and at the largest space-ground baselines the spike vanishes, proving that the scattering disk is resolved. Such behavior enables us to estimate angular diameter θ_H of the scattering disk. Fig. 4.5 illustrates dependence of visibility amplitude versus baseline projection for several pulsars observed with RadioAstron. Scattering parameters for these pulsars are presented in the Table 4.3.

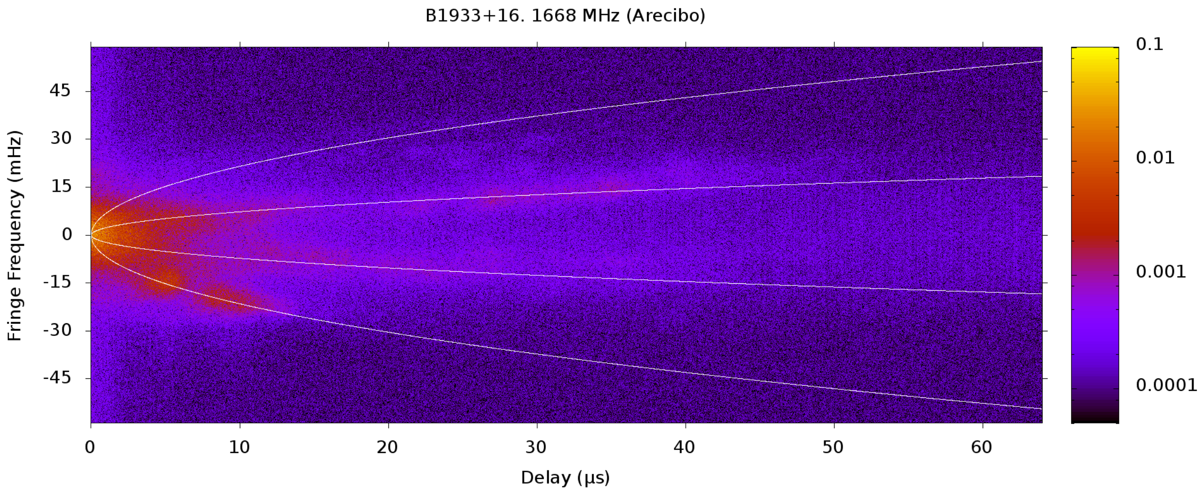

Fig. 4.4. Secondary spectrum for PSR B1933+16 at a frequency of 1668 MHz. Two parabolic arcs in the figure indicate on presence of two effective scattering screens between the observer and the pulsar.

Pulsar B1933+16 was observed simultaneously at two frequency ranges 316 and 1668 MHz during 1.5 hours on August 1 2013. Observations were supported by the Westerbork Synthesis Array (WSRT), Arecibo 300-m radio telescope and by 32-m telescopes in Torun (Poland) and Svetloe (IPA, Russia).

Figure 4.4 shows secondary spectrum for the PSR B1933+16. It was constructed by two dimensional Fourier transform from dynamic autospectrum obtained at Arecibo radio telescope. There are two well defined parabolic arcs in the figure. Such arcs were first detected and analyzed by Stinebring in 2001.

Curvature of the arc is connected by the simple formula with the distance to the scattering screen. Therefore, there are two such screens between the observer and the pulsar at distances of 1.3 and 3.1 kpc.

Fig. 4.5. Visibility amplitude versus baseline projection expressed in millions of wavelengths (Mλ). Pulsar B1641-45 (a) — solid line presents solution for scattering disk diameter of 27 mas; pulsar 1749-28 (b); pulsar B1933+16 (c) - 316 MHz, baseline WSRT-RadioAstron; B1933+16 (d) — 1668 MHz, baseline Arecibo — RadioAstron (triangles), and Arecibo-Svetloe (circles). Solid symbols and line correspond to upper sub-band, open symbols and dashed line correspond to lower sub-band.

In this study we have investigated distribution of scattering plasma in the direction to four pulsars B0329+54, B1641-45, B1749-28 and B1933+16, located in different directions in the Galaxy. Angular diameters of scattering disks were measured through visibility amplitude versus baseline dependence. Pulse time broadening was estimated as well by analyzing visibility function structure along delay coordinate. Distances to the effective scattering screens were estimated through the comparison of angular and time broadening. All results are collected in the Table 4.x. Model of uniform distribution of scattering plasma does not suit to any of the pulsar. Detected scattering layers of plasma for several pulsars were identified with real astronomical objects such as G339.1-04 (PSR B1641-45) and G0.55-0.85 (PSR B1749-28).

Table 4.3. Measured scattering parameters. Columns are as follows: (1) pulsar name, (2) number of cannels N_{ch}, (3) sampling rate of the correlator output ⍰t, (4) integration time for visibility ⍰T, (5) scintillation time ⍰t_{sc}, (6) decorrelation bandwidth ⍰⍰$_d$, (7) pulse broadening

time τ_{SC}, (8) diameter of scattering disk θ_H, (9) galactic coordinates *l,b,* (10) distance to the pulsar *D*, (11) distance to the scattering screen *d*.

Pulsar	N_{ch}	Δt, (s)	ΔT, (s)	Δt_{sc}, (s)	$\Delta\nu_d$, (kHz)	τ_{SC}, (µs)	θ_H, (mas)	*l, b,* (°)	D, (kpc)	d, (kpc)
B1641-45	16384	0.45	115	0.20 (0.05)	0.062 (0.002)	2600 (100)	27 (5)	339.2, -0.2	4.9	3.0
B1749-28	256	5.62	225	220 (20)	410 (100)	310 (0.040)	0.5 (0.2)	1.54, -0.96	1.3	0.95
B1933+16	8192	0.35	250	–	0.25 (0.15)	600 (400)	12.3 (0.6)	52.4, -2.1	3.7	2.6
B1933+16	2048	0.35	250	41.6 (0.5)	50.4 (1.1)	3.2 (0.1)	0.84 (0.04)	52.4, -2.1	3.7	2.7 [1.3;3.1]
B0329+54	2048	0.71	70	102	7 (2)	12 (3)	4.8 (0.8)	145 -1.2	1.0	0.5

4.3. ***PSR B0329+54: statistics of substructure discovered within the scattering disk on RadioAstron baselines of up to 235000 km***

Fine structure within the scattering disk of PSR B0329+54 was discovered in observations with RadioAstron space-ground interferometer at baseline projections from 60000 km to 235000 km. The observations were performed at 324 MHz with the support from 110-m Green Bank Telescope during four successive days in November 2012. The interferometric visibility on such long baselines takes the form of random phase and amplitude variations. The appearance of the interferometric response in delay/fringe-rate domain is shown in Figure 4.3. Visibility function forms a localized, extended region around the origin, composed of many random spikes. We characterize the shape of this region using averages and correlation functions. Interferometric visibility $V_{AB}(\tau, f_{max})$ is our fundamental observable (see section 4.2 for definition). We selected for our analysis cross-correlation between squared modulus of $V_{AB}(\tau, f_{max})$ obtained in two polarization channels (LCP and RCP). Example of such cross-correlation function $K_{RL}(\Delta\tau)$ is shown in Figure 4.7. One can see that there are two time scales in the CCF. We argue theoretically that such shape may be given by the average envelope of the impulse-response function of interstellar scattering, that has two different exponential scales:

$$G(\tau)=A_1 k_1 exp(-k_1 \tau)+A_2 k_2 exp(-k_2 \tau).$$

Grey solid line in Figure 4.7 shows our fit for a given observing scan. Such fitting was done for all our observations, and results for amplitude *A* and time scales $\tau=1/k$ are presented in Figure 4.8.

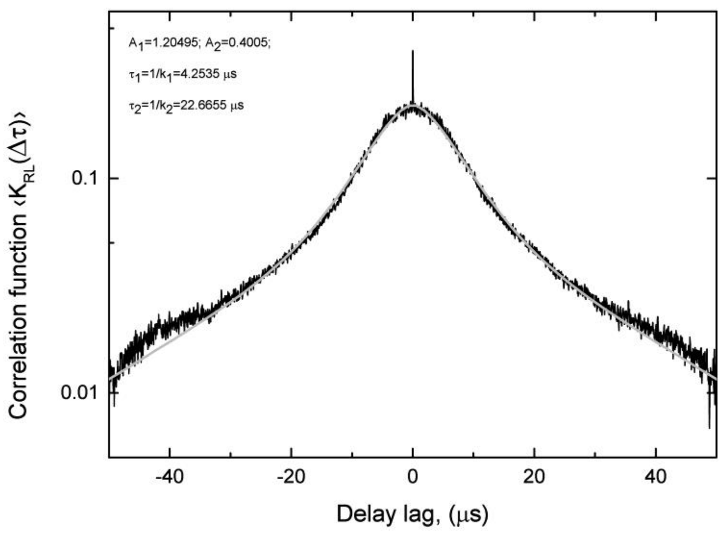

Fig. 4.7. *Example of cross-correlation function $K_{RL}(\Delta\tau)$ averaged over 570 seconds. Solid grey line represents two-exponential fit.*

Fig. 4.8. Top: distribution of long and short timescales for exponential scales detected in $K_{RL}(\Delta\tau)$. Bottom: distributions of magnitudes of long and short timescales.

It was found that impulse-response function contains two time scales 4.1 μs and 23 μs with ratio of amplitudes A_1/A_2=0.38. These average values do not vary notably with the baseline projections.

Two scales of scattering may be a consequence of a variety of factors. One explanation is anisotropic scattering. For this case with measured ratio k_2/k_1=5.5, ratio of scattering angles must be θ_2/θ_1=7.4, ratio of amplitudes must be 0.40, which is close to measured value. However, four days of observations with variety of orientation for space-ground baselines do not show anisotropy.

A second explanation is the complicated structure observed within dynamic spectra and called «scintillation arcs» (see Figure 4.4). Recently, it has been suggested that this structure arises from interference among sub-images, resulting from refraction by interstellar reconnection sheets. This complicated structure produces time and frequency variations on a wide range of scales. However, we do not observe scintillation arcs in the secondary spectrum of B0329+54 from our observations with the GBT. Future observations with RadioAstron for other bright pulsars may help to understand the puzzle of two time-scale scattering.

4.4 Studies of the Nearby, Turbulent Interstellar Plasma

We carried out observations of pulsar PSR B1919+21 at 324 MHz to study the distribution of interstellar plasma in the direction of this pulsar. Pulsar B1919 + 21 is a strong pulsar. It lies at galactic latitude 55^0 and longitude 3.5^0. Its dispersion measure is DM = 12.43 pc/cm^3. The Cordes & Lazio (2003) model as indicates that the pulsar distance is 1 kpc. Measurements of this pulsar's proper motion yielded $\mu_\alpha = 17 \pm 4$ mas/yr and $\mu_\beta = 32 \pm 6$ mas/yr (Zou et al. 2005). Separation of the effects of the close and distant medium it is required an availability of high spatial resolution, which in our observations was provided by our space-ground interferometer.

Observations of PSR B1919+21 were conducted using the Radioastron 10-m space radio telescope together with 110-m Green Bank (GBT) and 14*25-m Westerbork (WSRT) telescopes. All telescopes recorded the frequency band from 316 to 332 MHz, with one-bit quantization for space telescope data, and two-bit quantization for ground telescopes. The primary data processing was done using the ASC correlator (Andrianov et al. 2014) with incoherent dedispersion. Data were correlated with 512 spectral channels in two selected windows: on pulse and off pulse, the width of each window was 40 ms (3% of pulsar period, P = 1.337 c). An on-pulse window was centered on the maximum of the average profile, and an off-pulse window was selected at half the pulsar period from the on-pulse window. The projected space-ground interferometer baseline was 60000 km.

Figure 4.8 shows spectra of several strong pulses separated in time, with time increasing from bottom to top in the figure. Two scales of structure are visible in the spectra: small-scale structure with a frequency scale of about 400 kHz, and large-scale structure with frequency scale of about 1500 kHz. These scales are the approximate full width at half-maximum amplitude of the features. At smaller separations in time (as in spectra (a) and (b) in the figure, separated by 11 s), the fine structure is the same. Over longer separations (as in spectra (b) and (c), separated by 200 s) the fine structure changes, but the large-scale structure retains its shape.

A correlation analysis of the dynamic spectra provides the scales of scintillation in time, t_{dif} , and in frequency, f_{dif} .We obtained scales: $f_{1,dif}=330$ kHz and $f_{1,dif}=700$ kHz (half-width at the half-amplitude level), with amplitudes of 0.84 and 0.15 for the small- and large-scale structures, respectively. These structures are caused by scattering at the far and near layers of interstellar plasma.

For our ground baseline we used the usual procedure of calculation of the ACF, because the influence of noise was small and because, in addition, it was necessary to eliminate the influence of the ionosphere. For the space baseline, we calculated the ACF as the modulus of the average correlation function from the complex cross-spectra. This procedure is required when the contribution of the noise is greater than or comparable to the signal level, and when ionospheric effects are small, as was the case for our space baseline. Otherwise, the noise contribution will distort the ACF.

Analysis of the spatial coherence function for the space-ground baseline (RA-GB) yielded the scattering angle in the observer plane: $\theta_{scat}=0.7$mas. An analysis of the time-frequency correlation function for weak scintillations yielded the angle of refraction in the direction to the pulsar: $\theta_{ref}=120$ mas and the distance to the prism $Z_{prism}<1.3$ pc.

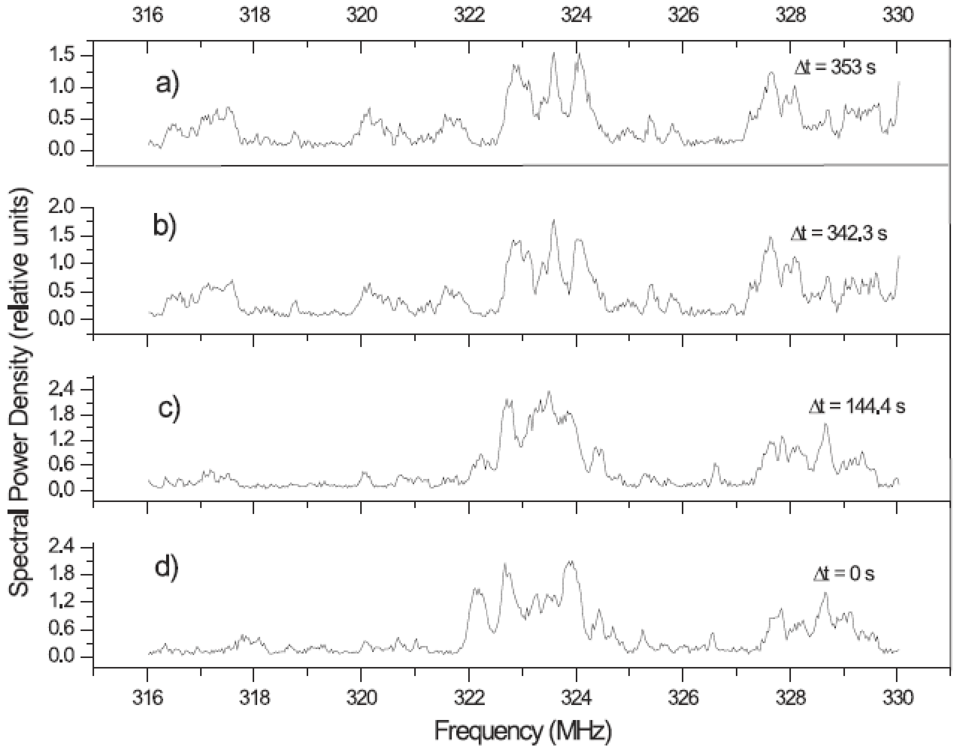

Fig. 4.8. Spectra of individual pulses of the pulsar, separated in time by the specified number of seconds from the bottom spectrum.

For a space interferometer using interferometric visibility function, we define the structural function as:

$$[illegible]$$

Figure 4.9 shows average time (upper) and frequency (lower) structure functions (SF) for our ground baseline on log-log axes. An arrow marks the break in the structure function at a frequency lag of 300 kHz. Time and frequency SF slopes differ by about a factor of 2 (for scales up to 250 KHz). $\beta_1 = 0.9 \pm 0.0$ for frequency structure functions and $\beta_2 = 1.73 \pm 0.0$ for time structure functions. This relation between frequency and time structure functions corresponds to the diffractive model of scintillation Shishov et al. (2003). The power-law index of the spectrum of density inhomogeneities n responsible for scattering is connected with the index of SF(t) through the relation $n=\beta_{2}+2=37$.

Figure 4.10 shows the average frequency structure functions for the ground (squares) and space-ground (circles) baselines at zero time shift. Evidently the levels of the SF differ by about 0.2. This corresponds to the relative contribution of two frequency scales in the scintillation spectra. The ratio of their amplitudes is consistent with the fitting the sum of two components into the average frequency correlation function for the ground baseline. The space-ground baseline shows no break in the structure function. This structure function displays the small-scale component of the spectra, with a relative amplitude of 0.8.

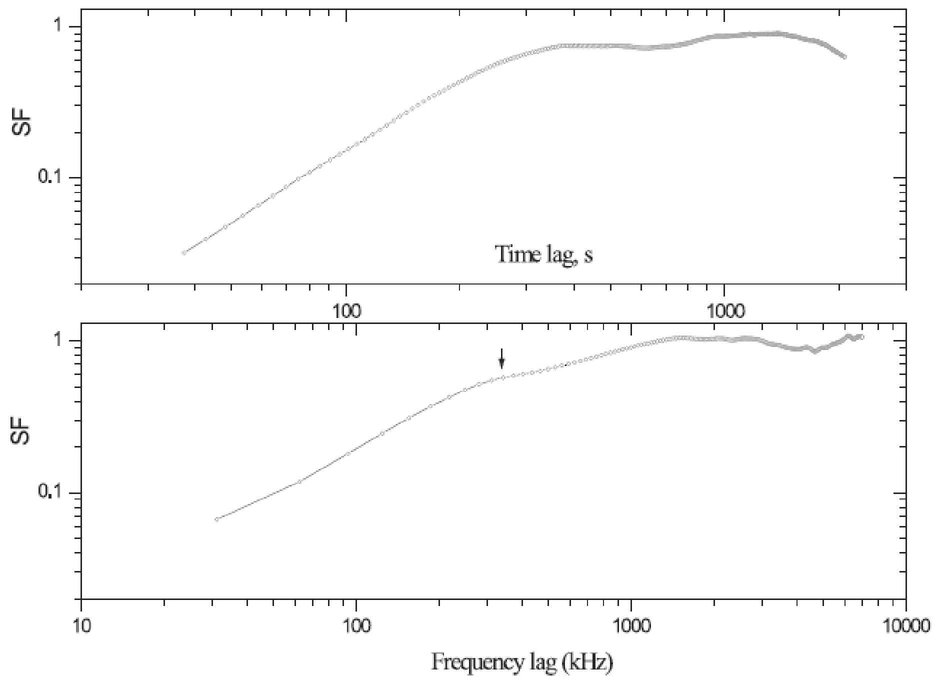

Fig. 4.9. Average time (upper) and frequency (lower) structure functions (SF) for Green Bank - Westerbork (GB-WB) baseline, presented on a log-log scale. The arrow marks the frequency lag of the observed break in the structure function, 300 kHz.

Analysis of frequency and time correlation functions and structure functions provide an estimate of the spatial distribution of interstellar plasma along the line of sight. We show that the observations indicate the existence of two screens in this direction: the first screen is located at a distance of about 440 pc from the observer and has the largest effects on the diffractive pulsar scintillations; the second screen is much closer, at a distance of about 0.13 pc, and corresponds to weak scintillation. The Fresnel scale is equal to 2.5*10^9 cm. Moreover, a cosmic prism is located behind the closest screen, leading to a drift of the diffraction pattern with a speed of 1.5 MHz / 1000 s in the dynamic spectrum. We have estimated the refraction angle of this prism as $\theta_{ref} = 120$ mas, and obtained an upper limit for the distance to the prism: $Z_{prism} < 1.3$ pc. Analysis of the spatial coherence function for the space-ground baseline (RA-GB) allowed us to estimate the scattering angle in the observer plane: $\theta_{scat} = 0.7$ mas. From temporal and frequency structure functions analysis we find for the index of interstellar plasma electron density fluctuations as n = 3.73.

This model follows the same structure as the model that was used for our scintillation studies of B0950+08 pulsar Smirnova et al. (2014). However, in this case the distance to the phase screen 1 is considerably greater, and characteristic scattering angle θ_{scat} also significantly larger, so that for PSR B1919+21 the scintillations are strong (and saturated).

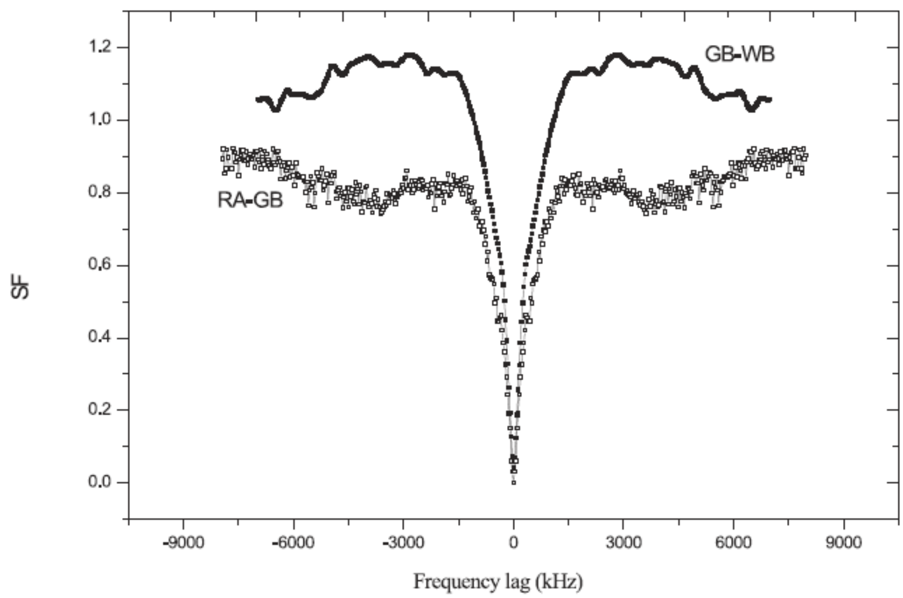

Fig. 4.10. Normalized frequency structure functions for ground (GB-WB) and space-ground (RA-GB) baselines**.**

5. RadioAstron study of galactic and extragalactic water masers

5.1 First space-ground detection of extragalactic megamaser: NGC 4258

RadioAstron has detected water maser emission from the circumnuclear disk of NGC4258 galaxy. NGC4258 (also known as Messier 106) is a spiral galaxy (Seyfert 2 type) located at the distance of 7.6 Mpc in the constellation Canes Venatici. The H_2O Megamaser NGC4258 is a prototype object with maser spots tracing the accretion disk around a supermassive black hole. The pumping is provided by the influence of X-ray emission from the center of the galaxy on the disk material. The existence of multiple components is explained by turbulence and instabilities in the disk. Interferometric signals were obtained with the space radio telescope (SRT) Spektr-R of the RadioAstron project and two ground facilities, the 100-m radio telescope in Green-Bank (USA) and the 32-m radio telescope in Torun (Poland) on 18 December 2014 (Figure 1). The spectrum in the figure shows a 30 minute integration. The extremely small spread among the fringe phases with velocity shows how remarkably thin the actual distribution of masers in the accretion disk is. The projected baseline length was up to 2 Earth diameters, corresponding to a fringe spacing of about 110 μas.

NGC3079, the second water megamaser source detected with RadioAstron, is a spiral galaxy (Seyfert 2 type) located at the distance of ~16-20 Mpc away toward the constellation Ursa Major. NGC 3079 contains one of the most luminous 22 GHz H_2O megamasers. The H_2O maser emission of NGC 3079 has been interpreted as originating in a circumnuclear disk (?) or might be related to shock passing through nuclear ISM because of superstarbursts (?).

Observations were conducted on 14 November 2014. The projected baseline length was up to 2.3 Earth diameters, corresponding to a fringe spacing of about 95 μas (Figure 2).

This first extragalactic detections suggests that H_2O Megamasers can be successfully studied with RadioAstron and that high resolution SVLBI imaging of H_2O Megamasers is possible leading to a detailed analysis of circumnuclear disks in other galaxies.

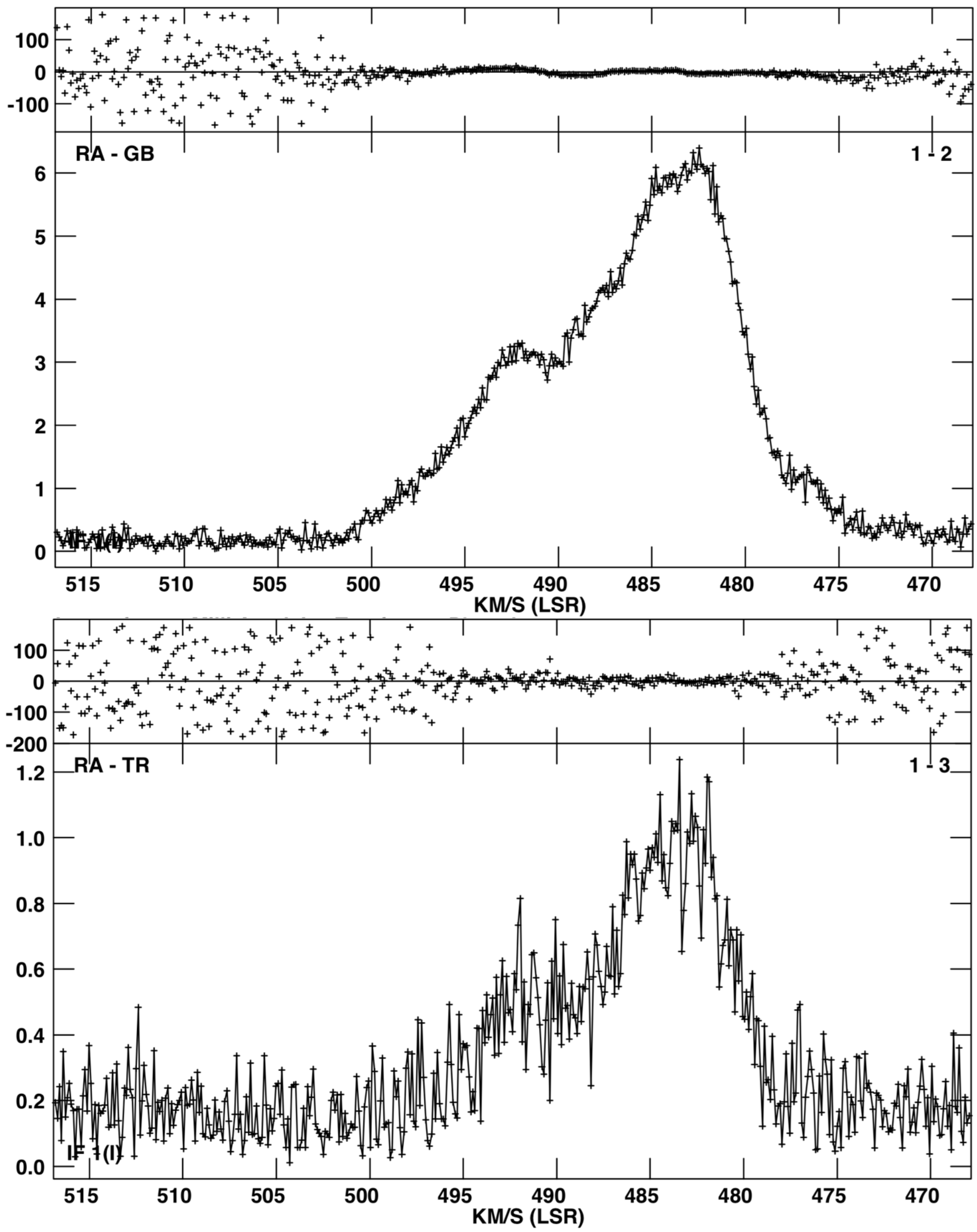

Fig. 5.1: Cross-correlation spectra of Megamaser emission in the galaxy NGC4258 obtained on space-ground baselines to the 100-m radio telescope in Green Bank (top) and 32-m radio telescope in Torun (bottom). The plots shows amplitude in arbitrary units and phase in degrees versus velocity in km/s recalculated to the LSR rest frame. The phase slope has been removed for this presentation. Fringe detections with high SNR occur in velocity ranges with small scatter in phase.

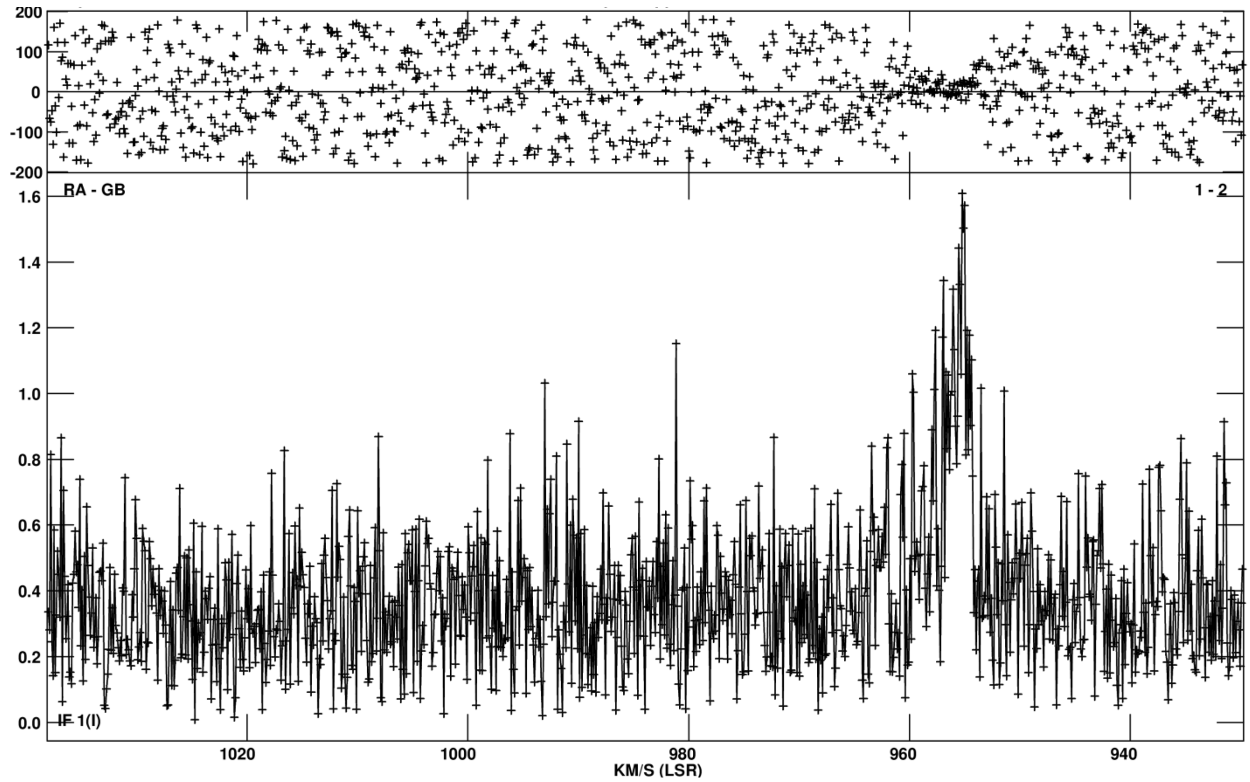

Fig. 5.2: Cross-correlation spectra of Megamaser emission in the galaxy NGC3079 obtained on space-ground baselines to the 100-m radio telescope in Green Bank. The plots shows amplitude in arbitrary units and phase in degrees versus velocity in km/s recalculated to the LSR rest frame. Fringe detections with high SNR occur in velocity ranges with small scatter in phase.

5.2. Water masers in star-forming regions of our Galaxy: Orion KL, W49 N, W3 (OH)

Successful detection of interferometric fringes from very compact water maser feature associated with the nearest and well-studied high-mass star-forming region Orion KL within the RadioAstron key science maser program is reported. Orion KL is a part of the Orion Nebular Cloud Complex and is located around 420 pc from the Sun. Active star formation occurs in this source, accompanied by a powerful maser radiation. Results of previous studies suggest that the compact maser spots are associated with the highly collimated outflow from the accreting young stellar object. The brightness temperature of the detected compact maser spot can exceed 10^{15} K. Correlated signals were obtained between the space and ground telescopes in two sessions. The 40-m radio telescope in Yebes (Spain), and the 32-m radio telescope in Torun (Poland) took part in the first session on 29 November 2013. The projected baseline length reached 3.5 Earth diameters, corresponding to a fringe spacing of ~63 µas. This corresponds to a linear size of about 3 solar diameters. In the second session (25 December 2013) Orion KL was detected on a baseline to the 26-m radio telescope in Hartebeesthoek (South Africa) with projected baseline of 2 Earth diameters. In both sessions V_{LSR} and line width of the detected maser detail were around 7.3 km/s and ~0.5 km/s, respectively. Recent observations of the most luminous water maser source in the Galaxy, star-forming region W49 N, resulted in a successful detection updating the RadioAstron record in angular resolution achieved in observations of cosmic masers. W49 N is located at a distance of about 11 kpc from the Sun in a distant part of the Perseus arm near the Solar circle. A correlated signal was obtained on 27 April 2015 between the space antenna and the two sensitive European ground facilities taking part in the experiment: the 100-m radio telescope in Effelsberg (Germany) and the 43-m radio telescope in Yebes (Spain). Projected baselines of the space-ground interferometer in the experiment reached up to about 9.7 Earth diameters, achieving a fringe-spacing resolution of ~23 µas.

A re-analysis of early RadioAstron observations at the ASC correlator has delivered a positive result for the bright water maser complex toward the TW object located ∼6 arcseconds to the east of the ultracompact H II region . A correlated signal was detected between the space antenna and the 100-m ground radio telescope in Effelsberg (Germany) and 40-m radio telescope in Yebes (Spain). Projected baselines of the space-ground interferometer in the experiment reached up to 3.8 Earth diameters (about 48,000 km), achieving a fringe-spacing resolution of ~58 µas.

The collected data on water masers are used to study structure and physical characteristics of the star forming regions in our Galaxy, impose tight limits on the sizes of individual maser spots, estimate brightness temperatures and provide the necessary input for the studies of their pumping mechanisms.

5.3. First imaging of water masers with RadioAstron.

A RadioAstron imaging of a water maser in the star-forming region W3 IRS5 took place on 17 October 2013 with participation of the European VLBI Network (EVN) including the Russian network "Quasar". Interferometric signals have been detected up to 6 Earth diameters delivering a record angular resolution of 36 µas for water masers. This corresponds to linear resolution of $\sim 10^7$ km. The space-ground interferometric image of the bright maser component in W3 IRS5 is shown in the left panel of Figure 3. The ground-only image has an extended structure, resolved out with the space-ground RadioAstron baselines except for a very compact peak visible up to the 6 Earth diameters. A joint analysis of the RadioAstron data and results of Japanese VERA interferometer monitoring allows international team of scientists to identify locations of the most compact maser emission (right panel, Figure 5.3).

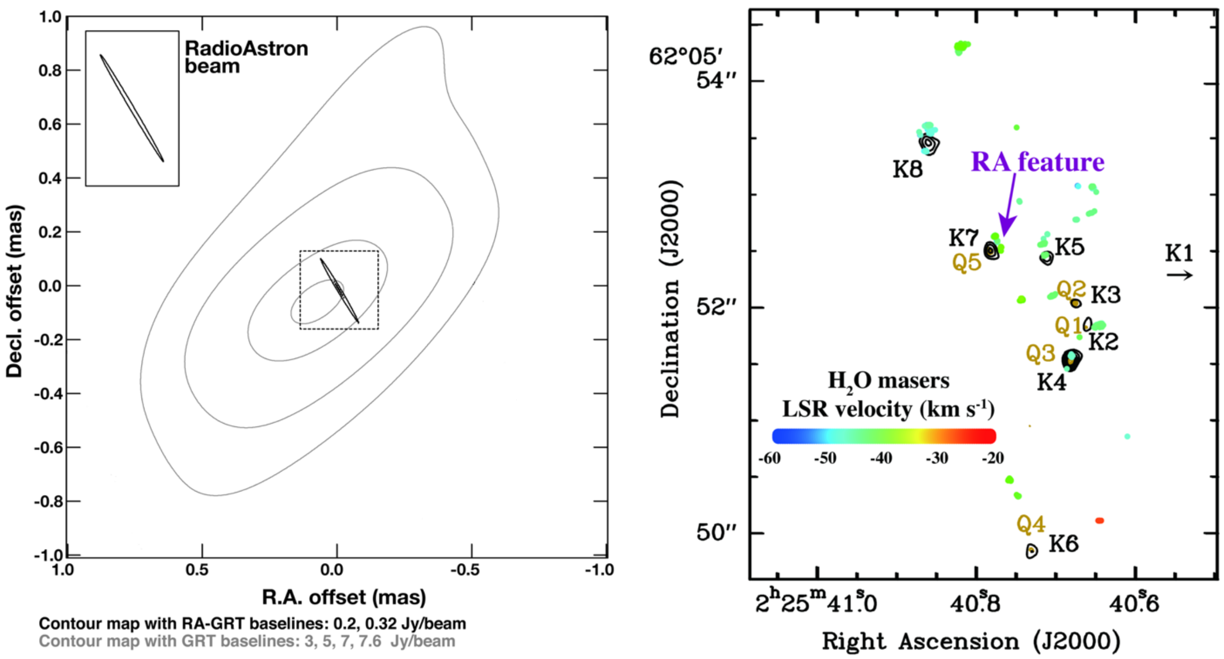

Fig. 5.2: W3 IRS5 left: contour map of the brightest H_2O spot detected in RadioAstron-EVN session on 17 October 2013. The image created in the narrow velocity range (0.1 km/s) corresponds to the peak spectral channel. The grey and black contours indicate the maser brightness distribution from RadioAstorn and ground-only data, respectively. The synthesized RadioAstron-EVN beam is displayed at the top-left corner of the map. Note that side lobes at the level up to 60 % of the real central brightest peak are omitted to avoid confusion. Right panel shows distribution of H_2O maser spots from W3 IRS5 as seen by the Japanese VERA interferometer 48 days before the RadioAstorn observation. The brightest compact maser feature is the one detected by RadioAstron (magenta arrow). Brown and black contours indicated the brightness distributions of the 7-mm and 13-mm band continuum emission, respectively (van der Tak et al. 2005).

During four years of operation 135 maser observation sessions were conducted, and 31 sources were observed. The majority of masers observed in RA program are related to star-forming regions – 19 sources in total. 8 masers sources, in the envelopes of late-type stars were observed and 4 extragalactic masers in star-forming regions and circum-nuclear disks of external galaxies were observed.

Due to technical reasons the scientific data have been corrupted or lost in 10 sessions out of total 135. At the moment, positive detections are obtained in 25 sessions. Some scientific data is still under consideration at ASC LPI data processing center. The final detection rate is likely to be higher.

6. Conclusions

6.1. We present observations of the quasar 3C 273, made with the space VLBI mission RadioAstron on baselines up to 171,000 km, which directly reveal the presence of angular structure as small as 26 µas (2.7 light months) and brightness temperature in excess of 10^{13} K. These measurements challenge our understanding of the non-thermal continuum emission in the vicinity of supermassive black holes and require a much higher Doppler factor than what is determined from jet apparent kinematics.

Besides 3C273, brightness temperature is measured for many other sources within RadioAstron AGN survey. Up to date, 150 quasars have been detected at ground-to-space baselines. The brightness temperature of their cores is measured to be up to 10^{14} K and even higher – inconsistent with previous and current findings of ground-based VLBI surveys.

6.2. Earth–space interferometry with RadioAstron provides the highest direct angular resolution ever achieved in astronomy at any wavelength. RadioAstron detections of the classic quasar 3C 273 on interferometric baselines up to 171,000 km suggest brightness temperatures exceeding expected limits from the "inverse-Compton catastrophe" by two orders of magnitude. We show that at 18 cm, these estimates most likely arise from refractive substructure introduced by scattering in the interstellar medium.

We use the scattering properties to estimate an intrinsic brightness temperature of 7×10^{12} K, which is consistent with expected theoretical limits, but which is ~15 times lower than estimates that neglect substructure. At 6.2 cm, the substructure influences the measured values appreciably but gives an estimated brightness temperature that is comparable to models that do not account for the substructure. At 1.35 cm, the substructure does not affect the extremely high inferred brightness temperatures, in excess of 10^{13} K . We also demonstrate that for a source having a Gaussian surface brightness profile, a single long baseline estimate of refractive substructure determines an absolute minimum brightness temperature, if the scattering properties along a given line of sight are known, and that this minimum accurately approximates the apparent brightness temperature over a wide range of total flux densities.

6.3. We present the first polarimetric space very long baseline interferometry (VLBI) imaging observations at 22 GHz. BL Lacertae was observed in 2013 November 10 with the RadioAstron space VLBI mission, including a ground array of 15 radio telescopes. The instrumental polarization of the space radio telescope is found to be less than 9%, demonstrating the polarimetric imaging capabilities of RadioAstron at 22 GHz. Ground–space fringes were obtained up to a projected baseline distance of 7.9 Earth diameters in length, allowing us to image the jet in BL Lacertae with a maximum angular resolution of 21 μas, the highest achieved to date.

We find evidence for emission upstream of the radio core, which may correspond to a recollimation shock at about 40 μas from the jet apex, in a pattern that includes other recollimation shocks at approximately 100 and 250 μas from the jet apex.

6.4. A space VLBI observation of high-redshift quasar TXS 0642+449 (OH 471), made at a wavelength of 18 cm (frequency of 1.6 GHz) as part of the early science programme (ESP) of the RadioAstron mission, is used here to test the polarimetric performance of the orbiting Space Radio Telescope (SRT) employed by the mission, to establish a methodology for making full Stokes polarimetry with space VLBI at 1.6 GHz, and to study the polarized emission in the target object on sub-milliarcsecond scales.

Polarization leakage of the SRT at 18 cm is found to be within 9% in amplitude, demonstrating the feasibility of high fidelity polarization imaging with RadioAstron at this wavelength. A polarimetric image of 0642+449 with a resolution of 0.8 mas (signifying an ~4 times improvement over ground VLBI observations at the same wavelength) is obtained. The image shows a compact core-jet structure with low (≈2%) polarization and predominantly transverse magnetic field in the nuclear region. The VLBI data also uncover a complex structure of the nuclear region, with two prominent features possibly corresponding to the jet base and a strong recollimation shock. The maximum brightness temperature at the jet base can be as high as 4×10^{13} K.

6.5. As result of the 22-hour long imaging experiment on 22 GHz, the central region of 3C 84 is resolved in a complex structure at sub-mas scale. The most prominent features are the core at the northern end of the jet and a bright component South of the core, which moves at sub-luminal speed along a curved trajectory connected to the core by a limb-brightened jet. The RadioAstron image shows substructure in these features at an unprecedented detail. For the first time a counter-jet is clearly visible at sub-parsec scale. The core is elongated in East-West direction implying a resolved structure at the angular resolution of about 50 μas, corresponding to about 500 Schwarzschild radii. The limb-brightened, well resolved jet and counter-jet can be seen right from the beginning. The bright spot inside the southern component is identified with the end of the limb-brightened jet. Its compactness indicates a very high brightness which is unusual for sub-luminal jets being observed at a large angle.

6.6. Substructure within the scattering disks was discovered in observations with the RadioAstron space-ground interferometer at large baseline projections (60000-250000 km). The substructure is produced by interstellar interferometer with the effective baseline of about one astronomical unit, and with effective angular resulution better than microarcsecond. It was proved by other investigators that interstellar interferometer acts also at other radio sources (not pulsars). This enable us to detect compact components in their structure. For example, such comact component was detected in the emission of radio sources SgrA*, located in the center of our Galaxy.

6.7. Angular diameters of scattering disk were measured for several distant pulsars using high angular resolution of the RadioAstron space-ground interferometer. Distances to the effective scattering screens were estimated for these objects. It was shown that detected layers of interstellar plasma are located close to the spiral arms or they are connected with known nebulae.

6.8. Using dedicated method of analysis, based on the treatment of stucture functions in spectral and time domains, we found scattering plasma layers close to the Sun. Such structure were postulated before to explain fast varbility of compact extragalactic sources, like AGN and quasars.

6.9. The average envelope of correlations of the visibility function shows two exponential scales. These two scales are present in the pulse-broadening function of the interstellar medium. It is possible that the longer tail arises from anisotropic scattering or from substructure at large angles.

6.10. Space-VLBI observations of the water and hydroxyl masers show that the bright details of the masers in galactic star-forming regions remain unresolved at baseline projections which considerably exceed Earth diameter. Record resolution for the maser observations at present are obtained for W49N water maser – 23 micro-arcsec at projected baseline 9.7 ED.

6.11. Very compact water maser features with the angular sizes of about 20 – 60 micro-arcseconds are registered in galactic star-forming regions. These correspond to linear sizes of about 5-10 million km (several solar diameters).

6.12. Estimates of the brightness temperatures for the ultracompact interstellar water maser features range from ~ 10^{13} to ~ 10^{16} K.

7. RadioAstron publications during 2014 - 2016 years.

Publications in refereed journals

- PSR B0329+54: Statistics of Substructure Discovered within the Scattering Disk on RadioAstron Baselines of up to 235,000 km.
  Gwinn, C. R., Popov, M. V., Bartel, N., Andrianov, A. S., Johnson, M. D., Joshi, B. C., Kardashev, N. S., Karuppusamy, R. , Kovalev, Y. Y., Kramer, M., Rudnitskii, A. G., Safutdinov, E. R., Shishov V. I., Smirnova T. V., Soglasnov V. A., Steinmassl, S. F., Zensus, J. A., & Zhuravlev, V. I.
  Astrophysical Journal, **822**, 2, 96 (2016)

- Иследование космической плазмы по данным РСДБ-наблюдений гигантских импульсов пульсара B0531+21 в проекте "РадиоАстрон".
  Рудницкий, А. Г., Каруппусами, Р., Попов, М. В., & Согласнов, В. А.
  Астрономический Ж., **93**, 167 (2016)
  Studies of Cosmic Plasma using RadioAstron VLBI Observations of Giant Pulses of the Pulsar B0531+21.
  Rudnitskiy, A. G, Karuppusamy, R., Popov, M. V., & Soglasnov, V. A.
  Astronomy Reports, **60**, 211 (2016)

- Probing the Innermost Regions of AGN Jets and Their Magnetic Fields with RadioAstron. I. Imaging BL Lacertae at 21 Microarcsecond Resolution.
  Gomez, J. L., Lobanov, A. P., Bruni, G., Kovalev, Y. Y., Marscher, A. P., Jorstad, S. G., Mizuno, Y., Bach, U., Sokolovsky, K. V., Anderson, J. M., Galindo, P., Kardashev, N. S., & Lisakov, M. M.
  Astrophysical Journal, **817**, 96 (2016)

- RadioAstron Observations of the Quasar 3C273: a Challenge to the Brightness Temperature Limit.
  Kovalev, Y. Y., Kardashev, N. S., Kellermann, K. I., Lobanov, A. P., Johnson, M. D., Gurvits, L. I., Voitsik, P. A., Zensus, J. A., Anderson, J. M., Bach, U., Jauncey, D. L., Ghigo, F., Ghosh, T., Kraus, A., Kovalev, Yu. A., Lisakov, M. M., Petrov, L. Yu., Romney, J. D., Salter, C. J., & Sokolovsky, K. V.
  Astrophysical Journal Letters, **820**, L9 (2016)

- Extreme Brightness Temperatures and Refractive Substructure in 3C273 with RadioAstron.
  Johnson, M. D., Kovalev, Y. Y., Gwinn, C. R., Gurvits, L. I., Narayan, R., Macquart, J. P., Jauncey, D. L., Voitsik, P. A., Anderson, J. M., Sokolovsky, K. V., & Lisakov, M. M.
  Astrophysical Journal Letters, **820**, L10 (2016)
- RadioAstron Space VLBI Imaging of Polarized Radio Emission in the High-Redshift Quasar 0642+449 at 1.6 GHz.
  Lobanov, A. P., Gomez, J. L., Bruni, G., Kovalev, Y. Y., Anderson, J., Bach, U., Kraus, A., Zensus, J. A., Lisakov, M. M., Sokolovsky, K. V., & Voytsik, P. A.
  Astronomy & Astrophysics, **583**, A100 (2015)

- Результаты испытаний радиоинтерферометра с нулевой базой в проекте "Радиоастрон".
  Бирюков, А. В.
  Космические исследования, **53**, 183 (2015)
  Test Results of Radio Interferometer with Zero Base in the RadioAstron Project.
  Biryukov, A. V.

Cosmic Research, **53**, 171 (2015)

- Формат данных и моды наблюдений интерферометра "Радиоастрон".
  Андреянов, В. В.
  Космические исследования, **53**, 195 (2015)
  Data Format and Observational Modes for the RadioAstron Interferometer.
  Andreyanov, V. V.
  Cosmic Research, **53**, 182 (2015)

- Управление и контроль функционирования бортового комплекса научной аппаратуры космического радиотелескопа.
  Бургин, М. С., Войцик, П. А., Кутькин, А. М., Лисаков, М. М., Миронова, Е. Н., Соколовский, К. В., & Фадеев Е. Н.
  Космические исследования, **53**, 199 (2015)
  Monitoring and Control of Onboard Scientific Equipment of the Space Radio Telescope.
  Burgin, M. S., Voytsik, P. A., Kutkin, A. M., Lisakov, M. M., Mironova, E. N., Sokolovsky, K. V., & Fadeev, E. N.
  Cosmic Research, **53**, 186 (2015)
- Исследование бортовой квантовой шкалы времени в условиях орбитального полета космического радиотелескопа проекта "Радиоастрон".
  Зиновьев, А. Н.
  Космические исследования, **53**, 207 (2015)
  Investigation of Onboard Quantum Time Scale for Orbital Flight of a Space Radio Telescope (the RadioAstron Project).
  Zinoviev, A. N.

Cosmic Research, **53**, 193 (2015)

- Первая оценка величины инструментальной поляризации космического радиотелескопа "Радиоастрон" по результатам ранней научной программы наблюдений активных ядер галактик.
  Пащенко, И. Н., Ковалев, Ю. Ю., & Войцик, П. А.
  Космические исследования, **53**, 214 (2015)
  First Estimate of the Value of the Instrumental Polarization of the RadioAstron Space Radio Telescope Using the Results of an Early Scientific Program for Observing Active Galactic Nuclei.
  Pashchenko, I. N., Kovalev, Yu. Yu., & Voitsik, P. A.
  Cosmic Research, **53**, 199 (2015)

- Использование наземных РСДБ станций Евпатория-Симеиз-Пущино в проекте "Радиоастрон".
  Вольвач, А. Е., Костенко, В. И., Ларионов, М. Г., Вольвач, Л. Н., Муха, Д. М., Набатов, А. С., Резниченко, А. М., Каневский, Б. З., & Коваленко, А. В.
  Космические исследования, **53**, 225 (2015)
  Testing of the Ground-based VLBI Stations Yevpatoria-Simeiz-Pushchino of the RadioAstron Mission.
  Volvach, A. E., Kostenko, V. I., Larionov, M. G., Volvach, L. N., Mucha, D. M., Nabatov, A. S., Reznichenko, A. M., Kanevsky, B. Z., & Kovalenko, A. V.
  Cosmic Research, **53**, 209 (2015)

- Пакет fakerat в международном интерферометрическом проекте "Радиоастрон" со сверхдлинными наземно-космическими базами.
  Журавлев, В. И.
  Космические исследования, **53**, 231 (2015)

  Fakerat Software in the International Interferometric RadioAstron Project with very Long Ground-Space Bases.
  Zhuravlev, V. I.
  Cosmic Research, **53**, 216 (2015)

- Создание и развитие программного комплекса для планирования наблюдений в проекте "Радиоастрон".
  Якимов, В. Е.
  Космические исследования, **53**, 242 (2015)
  Creation and Development of the Software Complex for Scheduling Observations in the RadioAstron Project.
  Yakimov, V. E.
  Cosmic Research, **53**, 226 (2015)

- PSR B0329+54: Substructure in the Scatter-broadened Image Discovered with RadioAstron on Baselines of up to 235,000 km.
  Popov, M. V., Andrianov, A. S., Bartel, N., Gwinn, C. R., Johnson, M. D., Joshi, B. C., Kardashev, N. S., Karuppusamy, R., Kovalev, Y. Y., Kramer, M., Rudnitskii, A. G., Safutdinov, E. R., Shishov, V. I., Smirnova, T. V., Soglasnov, V. A., Zensus, J. A., & Zhuravlev, V. I.
  Astrophysical Journal, submitted; preprint arXiv:1501.04449 (2015)

- RadioAstron as a Target and as an Instrument: Enhancing the Space VLBI Mission’s Scientific Output.
  Duev, D.A., Zakhvatkin, D.A., Stepanyants, V.A., Calves, G. M., Pogrebenko, S.V., Gurvits, L.I., Cimo, G., & Bocanegra Bahamon, T.M.
  Astronomy & Astrophysics, **573**, A99 (2015)

- Измерение гравитационного красного смещения с помощью космического радиотелескопа "РадиоАстрон".
  Бирюков, А. В., Кауц, В. Л., Кулагин, В. В., Литвинов, Д. А., & Руденко, В. Н.
  Астрономический Ж., **91**, 887 (2014)
  Gravitational Redshift Test with the Space Radio Ttelescope "RadioAstron".
  Biriukov, A. V., Kauts, V. L., Kulagin, V. V., Litvinov, D. A., & Rudenko, V. N.
  Astronomy Reports, **58**, 783 (2014)

- Наземно-космический радиоинтерферометр "РАДИОАСТРОН".
  Андреянов, В. В., Кардашев, Н. С., & Хартов, В. В.
  Космические исследования, **52**, 353 (2014)
  Space-Ground Radio Interferometer RadioAstron.
  Andreyanov, V. V., Kardashev, N. S., & Khartov, V. V.
  Cosmic Research, **52**, 319 (2014)

- Особенности управления миссией "РАДИОАСТРОН".
  Хартов, В. В., Ширшаков, А. Е., Артюхов, М. И., Казакевич, Ю. В., Воробьев, А. З., Калашников, А. И., Погодин, А. В., Филиппова, Е. Н., &

Комовкин, С. В.

Космические исследования, **52**, 360-365 (2014)

Features of RadioAstron Mission Control.

Khartov, V. V., Shirshakov, A. E., Artyukhov, M. I., Kazakevich, Yu. V., Vorob'ev, A. Z., Kalashnikov, A. I., Pogodin, A. V., Filippova, E. N., & Komovkin, S. V.

Cosmic Research, **52**, 326 (2014)

- Проектирование орбиты космического аппарата "СПЕКТР-Р" для наземно-космического интерферометра .

  Кардашев, Н. С., Крейсман, Б. Б., Погодин, А. В., Пономарев, Ю. Н., Филиппова, Е. Н., & Шейхет, А. И.

  Космические исследования, **52**, 366 (2014)

  Orbit Design for the Spektr-R Spacecraft of the Ground-Space Interferometer.

  Kardashev, N. S., Kreisman, B. B., Pogodin, A. V., Ponomarev, Yu. N., Filippova, E. N., & Sheikhet, A. I.

  Cosmic Research, **52**, 332 (2014)

- Навигационное обеспечение научной миссии "РАДИОАСТРОН".

  Захваткин, М. В., Пономарев, Ю. Н., Степаньянц, В. А., Тучин, А. Г., & Заславский, Г. С.

  Космические исследования, **52**, 376 (2014)

  Navigation Support for the RadioAstron Mission.

  Zakhvatkin, M. V., Ponomarev, Yu. N., Stepan'yants, V. A., Tuchin, A. G., & Zaslavskiy, G. S.

  Cosmic Research, **52**, 342 (2014)

- Коррекция траектории движения космческого аппарата "СПЕКТР-Р".

  Заславский, Г. С., Степаньянц, В. А., Тучин, А. Г., Погодин, А. В., Филиппова, Е. Н., & Шейхет, А. И.

  Космические исследования, **52**, 387 (2014)

  Trajectory Correction of the Spektr-R Spacecraft Motion.

  Zaslavskiy, G. S., Stepan'yants, V. A., Tuchin, A. G., Pogodin, A. V., Filippova, E. N., & Sheikhet, A. I.

  Cosmic Research, **52**, 353 (2014)

- Работа системы ориентации космического аппарата "СПЕКТР-Р".

  Лисаков, М. М., Войнаков, С. М. Сыров, А. С., Соколов, В. Н., Добрынин, Д. А., Шатский, М. А., Камальдинова, Р. А., Сосновцев, В.В., Рябогин, Н. В., Вьюнитская, Т. Б., & Филиппова, Е. Н.

  Космические исследования, **52**, 399 (2014)

  Operation of the Spektr-R Orientation System.

  Lisakov, M. M., Voinakov, S. M., Syrov, A. S., Sokolov, V. N., Dobrynin, D. A., Shatsky, M. A., Kamaldinova, R. A., Sosnovtsev, V. V., Ryabogin, N. V., Vyunitskaya, T. B., & Filippova, E. N.

  Cosmic Research, **52**, 365 (2014)

- Функциональные ограничения на ориентацию бортовых и наземных средств в проекте "РадиоАстрон".

Войнаков, С. М., Филиппова, Е. Н., Шейхет, А. И., & Якимов, В. Е.
Космические исследования, **52**, 408 (2014)

Functional Restrictions on the Orientation of Onboard and Ground Methods in the RadioAstron Project.
Voinakov, S. M., Filippova, E. N., Sheikhet, A. I., & Yakimov, V. E.
Cosmic Research, **52**, 373 (2014)

- Вопросы обеспечения точности конструкции космического радиотелескопа проекта "РАДИОАСТРОН".
  Федорчук, С. Д., & Архипов, М. Ю.
  Космические исследования, **52**, 415 (2014)

  On the Assurance of the Design Accuracy of the Space Radio Telescope RadioAstron.
  Fedorchuk, S. D., & Arkhipov, M. Yu.
  Cosmic Research, **52**, 379 (2014)

- Комплекс работ по численному моделированию динамики конструкции космического радиотелескопа проекта "РАДИОАСТРОН".
  Архипов, М. Ю., & Телепнев, П. П.
  Космические исследования, **52**, 418 (2014)

  System of Works on Numerical Modeling of the dynamics of the Structure of the Space Radiotelescope in the RadioAstron Pproject .
  Arkhipov, M. Yu., & Telepnev, P. P.
  Cosmic Research, **52**, 382 (2014)

- Система обеспечения теплового режима космического радиотелескопа.
  Тулин, Д. В., Виноградов, И. С., Шабарчин, А. Ф., Привезенцев, А. С., &

Гончаров, К. А.

Космические исследования, **52**, 423 (2014)

System of Maintaining the Thermal Regime of a Space Radio Telescope.

Tulin, D. V., Vinogradov, I. S., Shabarchin, A. F., Privezentsev, A. S., & Goncharov, K. A.

Cosmic Research, **52**, 386 (2014)

- Численное моделирование температурных деформаций космического радиотелескопа"РАДИОАСТРОН".

  Архипов, М. Ю., Виноградов, И. С., Новиков, С. Б., & Федорчук, С. Д.

  Космические исследования, **52**, 428 (2014)

  Numerical Modeling of RadioAstron SRT Temperature Deformations.

  Arkhipov, M. Yu., Vinogradov, I. S., Novikov, S. B., & Fedorchuk, S. D.

  Cosmic Research, **52**, 391 (2014)

- Проект "РАДИОАСТРОН". Измерения и анализ основных параметров космического телескопав полете в 2011-2013 ГГ.

  Ковалев, Ю. А, Васильков, В. И., Попов, М. В., Согласнов, В. А., Войцик, П. А. Лисаков, М. М., Кутькин, А. М., Николаев, Н. Я., Нижепьский, Н. А., Жеканис, Г. В., & Цыбулев, П. Г.

  Космические исследования, **52**, 430 (2014)

  The RadioAstron Project: Measurements and Analysis of Basic Parameters of Space Telescope in Flight in 2011-2013.

  Kovalev, Yu. A., Vasil'kov, V. I., Popov, M. V., Soglasnov, V. A., Voitsik, P. A., Lisakov, M. M., Kut'kin, A. M., Nikolaev, N. Ya., Nizhel'skii, N. A., Zhekanis, G. V., & Tsybulev, P. G.

Cosmic Research, **52**, 393 (2014)

- Блок антенных облучателей для проекта "РАДИОАСТРОН".

  Турыгин М. С.

  Космические исследования, **52**, 440 (2014)

  Antenna Feed Unit for the RadioAstron Project.

  Turygin M. S.

  Cosmic Research, **52**, 403 (2014)

- "РАДИОАСТРОН": итоги выполнения ранней научной программы исследований объектов Вселенной со сверхвысоким угловым разрешением.

  Кардашев, Н. С., Алакоз, А. В., Ковалев, Ю. Ю., Попов, М. В., Соболев, А. М., & Соколовский, К. В.

  Вестник НПО им. С.А. Лавочкина, No.3, 4 (2014)

  Radioastron: Main Results of the Implementation of the Early Science Program in Studies of Astronomical Objects
  in the Universe with Ultra-High Angular Resolution.

  Kardashev, N. S., Alakoz, A. V., Kovalev, Y. Y., Popov, M. V., Sobolev, A. M., & Sokolovsky K. V.

  Solar System Research, **49**, No. 7, 573 (2015)

- Проектирование орбиты космического аппарата "СПЕКТР-Р" для наземно-космического интерферометра.

  Кардашев Н.С., Хартов В.В., Крейсман Б.Б., Погодин А.В., Пономарев Ю.Н., Филиппова Е.Н., Шейхет А.И.

"SPEKTR-R" Spacecraft Orbit Design for Ground-Space Interferometer.

Kardashev, N. 5., Khartov, V. V., Kreisman, B. B., Pogodin, A. V., Ponomarev, Yu. N., Filippova, E. N., & Sheikhet, A. I.

Вестник НПО им. С.А. Лавочкина, No.3, 37 (2014)

- Наземнная станция слежения. Проект "РАДИОАСТРОН".

  Каневский, Б. З., Смирнов, А. И., Сазанков, С. В., Белоусов, К. Г., Шацкая, М. В., Абрамов, А. А., Селиверстов, С. И., Лихачев, С. Ф., Федоров, Н. А., Коваленко, А. В., Черный, Р. А., Суворин, Д. И., Логвиненко, С. В., Орешко, В. В., Исаев Е. А., Думский, Д. В., Кирпиченков, А. И., Скрипкин, А. А., Коган, Б. Л., & Зелезецкий, А. Л.

  The Earth-based Tracking Station. "RADIOASTRON" Project.

  Kanevskiy, B. Z., Smirnov, A. I., Sazankov, S. V., Belousov, K. G., Shatskaya, M. V., Abramov, A. A., Seliverstov, S. I., Likhachev, S. F., Fedorov, N. A., Kovalenko, A. V., Cherny, R. A., Suvorin, D. I., Logvinenko, C. B., Oreshko, V. V., Isaev, E. A., Dumckiy, D. V., Kirpichenkov, A. I., Skripkin, A. A., Kogan, B. L., & Zelezetskiy, A. L.

  Вестник НПО им. С.А. Лавочкина, No.3, 47 (2014)

- Корреляционная обработка данных наземно-космического интерферометра "РАДИОАСТРОН".

  Андрианов, А. С., Гирин, И. А., Жаров, В. Е., Костенко, В. И., Лихачев, С. Ф., & Шацкая, М. В.

  Correlator of the FIAN Astro Space Center in "RADIOASTRON" Mission.

  Andrianov, A. S., Guirin, I. A., Jarov, V. E., Kostenko, V. I., Likhachev, S. F., & Shatskaya, M. V.

  Вестник НПО им. С.А. Лавочкина, No.3, 55 (2014)

- Система регистрации радиоастрономических данных.

  Белоусов, К. Г., Дронова, О. Б., Лихачев, С. Ф., & Чибисов, А.В.

  Device for Recording of Radioastronomical Data.

  Belousov, K. G., Dronova, O. B., Likhachev, 5. F., & Chibisov, A. V.

  Вестник НПО им. С.А. Лавочкина, No.3, 60 (2014)

- Развитие центра обработки научной информации проекта "РАДИОАСТРОН".

  Шацкая, М. В., Абрамов, А. А., Гирин, И. А., Костенко, В. И., Лихачев, С. Ф., Селиверстов, С .И., & Федоров, Н. А.

  Development of Data Processing Center of "RADIOASTRON" Project.

  Shatskaya, M. V., Abramov, A. A., Guirin, I. A., Kostenko, V. L, Likhachev, S. F., Seliverstov, S. I., & Fedorov, N. A.

  Вестник НПО им. С.А. Лавочкина, No.3, 65 (2014)

- Функциональные ограничения на ориентацию бортовых и наземных средств в проекте "РАДИОАСТРОН".

  Войнаков, С. М., Филиппова, Е. Н., Шейхет, А. И., & Якимов, В. Е.

  Functional Constraints for Orientation of Onboard and Ground Aids for "RADIOASTRON" Project.

  Voinakov, S. M., Filippova, E. N., Sheikhet, A. I., & Yakimov V. E.

  Вестник НПО им. С.А. Лавочкина, No.3, 85 (2014)

- К вопросу о численном моделировании динамики конструкции космического аппарата "СПЕКТР-Р".

  Архипов, М. Ю., Телепнев, П. П., & Кузнецов, Д. А.

  On the Question of Numerical Simulation of "SPEKTR-R" Spacecraft Structure

Dynamics.

Arhipov, M. Yu., Telepnev, P. P., Kuznetsov D. A.

Вестник НПО им. С.А. Лавочкина, No.3, 96 (2014)

- RadioAstron Studies of the Nearby, Turbulent Interstellar Plasma with the Longest Space-Ground Interferometer Baseline.

  Smirnova, T. V., Shishov, V. I., Popov, M. V., Gwinn, C. R., Anderson, J. M., Andrianov, A. S., Bartel, N., Deller, A., Johnson, M. D., Joshi, B. C., Kardashev, N. S., Karuppusamy, R., Kovalev, Y. Y., Kramer, M., Soglasnov, V. A., Zensus, J. A., Zhuravlev, V. I.

  Astrophysical Journal, **786**, 115 (2014)

Selected Proceedings of Conferences

- RadioAstron gravitational redshift experiment: status update.

  Litvinov, D. A., Bach, U., Bartel, N., Belousov, K. G., Bietenholz, M., Biriukov, A. V., Cimo, G., Duev, D. A., Gurvits, L. I., Gusev, A. V., Haas, R., Kauts, V. L., Kanevsky, B. Z., Kovalenko, A. V., Kronschnabl, G., Kulagin, V. V., Lindqvist, M., Molera, Calves, G., Neidhardt, A., Ploetz, C., Pogrebenko, S. V., Porayko, N. K., Rudenko, V. N., Smirnov, A. I., Sokolovsky, K. V., Stepanyants, V. A., Yang, J., & Zakhvatkin, M. V.

  Submitted to the 14th Marcel Grossmann Meeting Proceedings, arXiv:1605.05832 (2016)

- Measurement of the Gravitational Redshift Effect with RadioAstron Satellite.

  Birukov, A. V., Kauts, V. L., Litvinov, D. A., Porayko, N. K., & Rudenko, V. N.

  Proceedings to Recontres de Moriond 2015; preprint arXiv:1506.02238 (2015)

- Gravitational Redshift Experiment with the Space Radio Telescope RadioAstron.
  Litvinov, D., Bartel, N., Belousov, K., Bietenholz, M., Biriukov, A., Fionov, A., Gusev, A., Kauts, V.,
  Kovalenko, A., Kulagin, V., Poraiko, N., & Rudenko, V.
  Proceedings of the Journees 2014 "Systemes de reference spatio-temporels": Recent developments and prospects in ground-based and space astrometry, Pulkovo Observatory, St. Petersburg, Russia, 22-24 September 2014; preprint arXiv:1503.03641 (2015)

- Preliminary Results of Giant Pulse Investigations from Crab Pulsar with RadioAstron.
  Rudnitskiy, A. G., Popov, M. V., & Soglasnov, V. A.
  Proceedings of Science, EVN 2014, 065 (2015)

- Study of Scattering Material with RadioAstron-VLBI Observations.
  Andrianov, A., Smirnova, T. V., Shishov, V. I., Popov, M. V., Kardashev, N. S., Soglasnov, V. A.,
  Gwinn, C., Johnson, M., Bignall, H., Deller, A., & Kramer, M.
  Proceedings of Science, EVN 2014, 064 (2014)

- The Nuclear Structure of 3C84 with Space VLBI (RadioAstron) Observations.
  Giovannini, G., Orienti, M., Savolainen, T., Nagai, H., Giroletti, M., Hada, K., Bruni, G., Hodgson, J., Honma, M., Kino, M., Kovalev, Y. Y.; Krichbaum, T., Lee, S., Lobanov, A., Sohn, B., Sokolovsky, K., Voitsik, P., & Zensus, J. A.

Proceedings of Science, EVN 2014, 021 (2014); preprint arXiv:1504.01516 (2015)

- Space-VLBI with RadioAstron: new Correlator Capabilities at MPIfR.
  Bruni, G., Anderson, J.M., Alef, W., Lobanov, A., Zensus, J.A.
  Proceedings of Science, EVN 2014, 119 (2014); preprint arXiv:1502.06894 (2015)

- The RadioAstron Green Bank Earth Station.
  Ford, H. A., Anderson, R., Belousov, K., Brandt, J. J., Ford, J. M., Kanevsky, B., Kovalenko, A., Kovalev, Y. Y., Maddalena, R. J., Sergeev, S., Smirnov, A., Watts, G., & Weadon, T. L.
  Proceedings of the SPIE, **9145**, id. 91450B 11 pp. (2014)

- Space VLBI Mission RadioAstron: Development, Specifications, and early Results.
  Kovalev, Y. Y., Kardashev N. S., & RadioAstron collaboration
  Proceedings of Science, **40**, 1 (2012)

- RadioAstron Early Science Program.
  Space-VLBI AGN Survey: Strategy and First Results.
  Sokolovsky, K. V. for the RadioAstron AGN Early Science Working Group,
  Proceedings of Science, 11th EVN Symposium, 1 (2012)